Safety Analysis of Modern Heritage Masonry Buildings: Box-buildings in Recife, Brazil.

Jenner Carvalho[a], Javier Ortega[b], Paulo B. Lourenço[b*], Luís F. Ramos[b], Humberto Roman[a]

[a] Department of Civil Engineering, Federal University of Santa Catarina, Florianópolis, Brazil

[b] ISISE, Department of Civil Engineering, University of Minho, Guimarães, Portugal

* Correspondence to Paulo B. Lourenço, ISISE, Department of Civil Engineering, University of Minho, Campus de Azurém, Guimarães, 4800-058, Portugal; E-mail: pbl@civil.uminho.pt; Tel: +351 253 510 200

Abstract: Box-buildings are structural masonry buildings named as such because of their shape. There are around 5,000 of them in Recife, Brazil. This paper presents a safety analysis of one box-building that suffered collapse on December 2007. The research aims at quantifying the safety of this type of existing buildings and at better understanding their structural behavior to try to identify the reasons for the collapse. A finite element model was prepared and a set of nonlinear numerical analyses were performed. The results of the analyses show good agreement between the observed damage in the real building and the damage achieved numerically at the current condition (LF=1). The model thus seems to represent satisfactorily the real behavior of the building but the safety factor obtained seems too conservative and does not justify the collapse observed in reality. Since results show that the building should not have failed under normal working conditions, a collapse assessment about why the building fell is therefore provided and a sensitivity analysis was performed in order to understand the importance of the material parameters and their influence on the structural response of the building.

Keywords: Structural Failure; Building Collapse; Masonry Building; Testing; Finite Element Analysis; Safety Analysis; Sensitivity Analysis

Highlights:

- Finite element model of a structural masonry building in Recife that suffered collapse
- The safety of the buildings was quantified by a set of nonlinear analyses
- The safety factor obtained is too high to justify the collapse of the building under normal working conditions
- Demonstration that the foundation saturated masonry suffered critical deterioration
- Demonstration that compressive fracture energy can be important in justifying building collapse

Short Title: Safety Analysis of Box-buildings in Recife

1. Introduction

It is estimated that there are between 4,000 to 6,000 buildings constructed with the common characteristics of the so-called box-buildings in the Recife Metropolitan Region (RMR), Brazil. They are inhabited by more than 250,000 people, comprising approximately 10% of the population of the region. Up to 90% of these buildings seem to present some risk of collapse, with different severity, and a total of 230 of these buildings are classified as having high risk of collapse and have already been evacuated [de Melo, 2007]. Twelve box-buildings have collapsed over the past 20 years, causing a dozen casualties. Due to the large number of buildings and people involved, this situation has become one of the major urban problems in Recife. The problem affects generally low income families, which are mostly the inhabitants of these buildings. The inhabitants face problems such as the evacuation of buildings and relocation, and the fear to continue to live in an area where other buildings have collapsed.

There was a big rural exodus towards the cities during the 1970s, particularly in Brazil, and box-buildings arose at that time because of housing shortage, bringing great masses of workers which accumulated on the peripheries of the urban centers. These buildings are the result of speculative activities, with low cost and high speed construction with unskilled labor. The building development was made by non-experts interested only in the fast return of the investment, with no consideration of specific technical norms or standards, thus, critically reducing their safety coefficient. The main problems seem to be a poor choice of materials and the adoption of technically inadequate building solutions, followed by a fast progressive degradation process, with premature ageing and many damage manifestations.

Many research projects have been carried out in Brazil concerning this problem [Gusmão, 2009; Lourenço, 2011]. However, the characterization of the materials is

particularly difficult, given the low quality of the materials and the many factors which seem to be affecting them. The unsuitability of the masonry used in the buildings for a structural purpose was confirmed, proven to be insufficient to bear the stresses to which it is subjected to. Still, the anomalies encountered are not only a result of inadequate materials and defects in construction works but also are affected by the lack of maintenance and different environmental causes, such as moisture or chemical attacks. The reasons for the collapse are still unclear and no sound methodology to assess the safety and strengthen these buildings is available. Therefore, the main objective of the present work is to contribute to find an adequate solution to this problem.

It is common to see social housing in poor condition, in different countries. Efforts in rehabilitation and conservation need to also address this modern heritage which involves social housing and modern buildings, which are a part of the current urban landscape. Conservation engineering is a multidisciplinary approach that needs a full understanding of the materials and the structure, and aims at acquiring enough data to produce optimal interventions. Here, one box-building that suffered collapse is adopted as a case study of an experimental and numerical research in order to quantify the safety of this type of buildings and better understand their structural behavior. For this purpose, an extensive testing program was carried out by de Carvalho [2010], including non-destructive and minor destructive testing on the building, as well as laboratory testing.

The possibility of using sophisticated numerical models for the analysis of structures and for structural safety assessment has been highly enhanced in the recent years but performing a structural analysis of an existing construction remains a complex task, given the uncertainties about the material properties, the morphology of structural elements, the connection between structural elements, and the construction phases, among other aspects, see Lourenço [2002] and Lourenço et al. [2011]. For a deeper comprehension of the specific

purposes and challenges in the modelling of the mechanical behavior of an extremely heterogeneous material such as masonry, the reader is referred to Lourenço [1998] and Roca et al. [2010]. In this study, the structural assessment was carried out using the finite element method as the analysis tool. Moreover, given masonry inherent uncertainties, a sensitivity analysis was also carried out to understand the importance of each material parameter and its influence on the global structural response of the building.

2. Description of the Studied Building and Testing

The research is focused on one of the box-buildings of the residential complex *Sevilha*, in *Jaboatão dos Guarapes*, within the RMR. The residential complex is composed by four blocks of very similar characteristics. Block B partially collapsed on December 2007 and it was later demolished. Figure 1 shows the building after the collapse. Failure of the foundation masonry walls was observed. This collapse triggered the experimental and numerical research carried out by de Carvalho [2010]. The visual inspection and testing program described next was performed on the block C of the complex.

2.1. Characterization

The general features of the studied building correspond to the common features and characteristics of the box-buildings regarding appearance, structural system and materials. In the absence of documentation of the original project, an exhaustive visual inspection was performed comprising the roof and, especially, the foundations. In some cases, renderings were removed and openings were executed in order to observe and inspect the structural building elements.

The building is four-stories high and has a water reservoir on the top made in reinforced concrete, with a total height of 17 meters. The strong squared shape of the building

is only disrupted by the staircase, which is situated in the central part of the building and is set back further than the rest of the façade. The staircase also holds the entrance to the building and supports the water reservoir. The structure consists of unreinforced masonry walls, which supports the beam and block floor slabs and transfer the load to the foundation walls, executed also in masonry. The external walls are rendered with mortar and painted.

The architectural plans of the building are shown in Figure 2. The internal structural masonry walls act also as partition walls and define the layout of the building, which is quite regular and almost symmetric with respect to the two orthogonal axes. The plan has an H shape configuration with the staircase dividing it in two parts. There are four apartments per floor of small dimensions, around 55 m^2. The inter-story height is 2.60 m and the ground floor is elevated with respect to the outside ground level, meaning that it is necessary to climb four steps in order to access the building. The roof is covered with fiber cement sheeting and it is not accessible.

Figure 3 shows a construction detail from the foundations to the ground floor. The foundations are made using continuous reinforced concrete footings, with a width of 500 mm and a height of 150 mm, and unreinforced masonry walls. The masonry walls are built with hollow clay blocks with dimensions about 90 × 190 × 190 mm^3 with 8 holes positioned horizontally. They lay on their largest dimension, 190 mm, and the average thickness of the mortar bed joints is 30 mm, but it is very variable. The external mortar rendering has a variable thickness between 40 and 50 mm. No internal rendering is present and altogether, the masonry walls are around 230 mm thick. The depth of the ground water table is 0,75 m and, therefore, a significant part of the foundations is in direct contact with water. As there is no waterproofing, the first layers of the masonry are permanently saturated. Moreover, there is no sewage collector in the building and the water is contaminated, which may result in accelerated degradation of the mechanical properties of the blocks [de Oliveira, 2009].

Regarding the structure above ground, the structural unreinforced masonry walls are constructed with the same masonry units used in the foundations but lying on their smallest dimension, 90 mm. The thickness of the mortar bed joints varies between 20 and 30 mm, the external mortar rendering can reach up to 60 mm thickness, while the internal mortar rendering varies between 20 and 25 mm. Therefore, the overall thickness of the walls varies between 120 and 150 mm. The beam and block floor system is used for the floor slabs, consisting of prestressed concrete joists and hollow concrete tiles with an overall thickness of 200 mm. The spacing between joists is 450 mm. There are reinforced concrete tie-beams at every floor level.

2.2. Testing and obtained data

The investigation campaign performed on the building to assess the existing damage and to better understand its structural behavior is summarized in Figure 4. Non-destructive and minor destructive *in situ* tests were performed and 22 prisms samples were extracted from the building for further testing on the laboratory. Ten prisms were tested in the laboratory of the University of Minho, in Portugal, and twelve prisms were tested in the laboratory of SENAI-PE, in Brazil. Most of the parameters later used in the FEM model were determined from this extensive experimental research. A brief description of the tests most relevant for the present work is provided next. Further discussion on the results of the other tests can be found in de Carvalho [2010] and Ortega [2013].

The dynamic properties of the building (frequencies and mode shapes) obtained through dynamic identification were obtained under ambient vibration and later used to validate the FEM model. The data acquisition system consisted of several piezoelectric accelerometers and one acquisition unit. The sensors were located in the three upper floors in the two orthogonal directions within the horizontal plane, in order to capture the bending and

torsion modes. Three different set-ups were conducted and measurements were performed with an acquisition frequency of 200 Hz. The environmental conditions were also monitored and, since no abrupt changes were measured, it was assumed that the dynamic response of the structure was not affected by the environmental parameters. The modal identification method used was the Stochastic Subspace Identification (SSI). The results showed seven frequencies identified in the range from 4.0 to 7.5 Hz. The global dynamic response of the building is influenced by the central staircase, which is stiffer because of the material used. The building has a tendency to rotate while the central staircase remains almost fixed.

Regarding the laboratory investigation aimed at defining the characteristics of the materials, monotonic uniaxial compressive tests were performed on six purchased blocks of similar characteristics to those used in the box-buildings in order to have a first indication of the compressive strength of the material. The peak stress and the modulus of elasticity were obtained, distinguishing between saturated and non-saturated condition. The results were exceptionally low and, as expected, even lower for the saturated blocks. The average compressive strength obtained was 1.51 MPa for the non-saturated blocks and 0.97 MPa for the saturated blocks. The average moduli of elasticity obtained were 147.8 MPa and 111.2 MPa for the non-saturated and saturated blocks, respectively. Compressive tests were performed also on six mortar specimens extracted directly from the building, three of which were saturated. The average compressive strength measured was 5.23 MPa for the non-saturated specimens and 3.22 MPa for the saturated specimens.

With respect to the testing of the prisms extracted directly from the building, a large variability in the results was observed, probably due to the variability in the materials dimensions and the poor quality of the blocks. Nevertheless, average stress-strain relations were registered and the compressive strength and Young's modulus to be used in the subsequent analyses were obtained. Only six out of the ten prisms collected could be tested in

the laboratory of the University of Minho. Since some of the blocks are expected to be saturated in the building, an important distinction was made between saturated and non-saturated condition. Therefore, three of the prisms were immersed in water for 28 days prior to testing. The thickness of the prisms was remarkably variable and the average thickness of the mortar bed joint was assumed as 27 mm. Monotonic compressive tests were then performed on the prisms and from these tests, the compressive strength and the elasticity modulus were obtained. Table 1 presents the geometrical characteristics of the prisms and the results of the compressive strength tests, which were later used in the FEM model. The collapse of the prisms occurred right after the first detachment of the rendering, leading to a sudden failure. A very brittle behavior of the masonry was then verified, as cracking of the block occurred very close to the ultimate load. Figure 5 shows the failure modes of the prisms and the detachment of the rendering.

Laboratory testing confirmed that the mechanical properties of the materials were substantially lower when they are saturated. Also, the positive influence of the rendering in the compressive behavior was confirmed. However, the bond characterization between the rendering and the substrate using pull-off testing showed that the values obtained for bond strength do not meet the requirements established by the applicable standards.

3. Finite element model

The present research focuses on the safety assessment of one box-building. A numerical model was constructed to simulate the structural behavior of the building and to verify its safety. The model was made taken into consideration the geometrical and material data obtained from the inspection and testing campaign.

Masonry is a complex material to model due to the inherent anisotropy and variability of properties. Only a few authors implemented constitutive non-linear models able to consider

different strength and deformation capacity among the material axes for finite element analysis, e.g. Lourenço [2000] and Calderini and Lagomarsino [2008]. These models are not widely disseminated and can be hard to apply to traditional buildings given the difficulties to characterize the existing fabric with a high level of detail.

For this purpose, the material model adopted to represent the nonlinear behavior of the masonry in the analysis is a standard isotropic Total Strain Fixed Crack model, which describes the tensile and compressive behavior of the material with one stress-strain relationship and it was constructed using the DIANA software [TNO, 2011]. Like traditional smeared crack models, e.g. Rots [1988], the total strain based crack models follow a smeared approach for the fracture energy, but provide a more robust numerical algorithm. This model is very well suited for analyses which are predominantly governed by cracking or crushing of the material. The tension softening function selected is exponential and the compressive function selected to model the crushing behavior is parabolic. This software and constitutive model have been already successfully applied in previous analyses of complex masonry structures, e.g. Ramos and Lourenço [2004] and Lourenço et al. [2007].

All the structural elements were simulated as shell elements. The mesh includes quadrilateral isoparametric 8 nodes (CQ40S) shell elements, with two-by-two Gauss integration in the plane and seven-point Simpson integration in the thickness direction, and triangular isoparametric 6 nodes (CT30S) shell elements, with a three-point integration scheme in the plane and seven-point Simpson integration in the thickness direction. The areas are discretized in these two different elements depending on the geometry and because of the manipulation realized after the automatic generation of the mesh by DIANA, aiming at obtaining a better quality mesh. These curved shell elements are degenerated from a 3D formulation and are adopted here to reduce the degrees of freedom in a complete 3D analysis. This degeneration is based on two hypotheses: (i) normals to the mid-plane of the element

remain straight, but not necessarily perpendicular to it; and (ii) the normal stress component perpendicular to the mid-plane equals zero. This element, originally proposed by Ahmad et al. [1970] for the linear analysis of moderately thick shells, has been extensively used for the geometrical and nonlinear analysis of shell structures. The use of this element for successfully reproduce the nonlinear behavior of masonry walls has been validated in Lourenço [2000] and successfully used in previous work including Mendes and Lourenço [2009], Araujo et al. [2012], Ademovic et al. [2013] and Marques et al. [2013].

The elements at the base are fully restrained. The resulting generated mesh has 37,235 nodes and 13,199 elements, see Figure 6. The four different materials used in the numerical model are shown in Figure 7. Saturated masonry is used for the foundation walls, non-saturated masonry for the rest of the masonry walls, reinforced concrete is used for the tie-beams, stairs and water reservoir, and the beam and block floor system is used for the floor slabs. The total mass of the model is 1020 tonnes.

3.1. Calibration of the finite element model

The dynamic identification tests carried out in the building allowed obtaining the vibration modes and their frequencies. Therefore, the finite element model dynamic characteristics could be compared with the experimental ones. The parameters to be calibrated in the model were the elasticity modulus of both the saturated and the non-saturated masonry. The average elasticity modulus obtained from the compressive tests was 1168 MPa for the saturated masonry and 3307 MPa for the non-saturated masonry. These were the values used as reference for the calibration. Subsequent iterated reductions on these parameters were carried out and the frequency error of the three first mode shapes was calculated until the error was minimized. The optimized model, in comparison to the experimental value, has an average error only of 6,9%, see Table 2. The optimized parameters to be used in the analysis

are 1052 MPa for the saturated masonry and 2977 MPa for the non-saturated masonry, which means a 10% reduction of the original measured values in the tested prisms.

3.2. Material properties

Only the masonry is considered to present nonlinear behavior as all structural nonlinearities are expected to concentrate there. For the concrete, an elasticity modulus of 24 GPa and a Poisson's ratio of 0.2 were used. For the elastic properties of masonry, the elasticity modulus obtained from the dynamic calibration was used and the Poisson's ratio used was 0.13.

The masonry compressive strength is also determined from the compressive tests. According to Eurocode 8 [2004], the characteristic value to use in the analysis shall be the minimum between the minimum value obtained from tests and the mean value obtained from tests divided by the confidence factor, which in this case, assuming a level of knowledge 2 (normal knowledge) is 1.2.

The remaining nonlinear properties are computed directly from the compressive strength f_c and are based on recommendations given in Lourenço [2009], as detailed next. Table 3 present the nonlinear properties adopted for the analysis. The compressive fracture energy G_{fc} is obtained using a ductility factor d of 1.6 mm, which is the ratio between the fracture energy and the ultimate compressive strength. The tensile strength f_t is estimated at 1/10 of the compressive strength. Finally, an average value of 0.012 is adopted for the mode I fracture energy G_{fI} and a value of 0.05 is used for the shear retention factor β.

4. Structural analysis

The results obtained in the analyses are now presented. First, the safety analysis of the structure is presented, performed in order to determine the safety of this type of building and

understand its structural behavior, which is the primary objective of the present research. Second, the collapse assessment is presented, in which a series of analyses were performed in order to evaluate why the building fell in reality and a hypothetical explanation of the collapse is suggested, where the possible long-term effects on the saturated masonry were taken into account. Finally, the results from the sensitivity analysis are presented, carried out in order to understand the importance of the material parameters and their influence on the global structural response of the building. A thorough and complete discussion on the results of all analyses can be found in Ortega [2013].

4.1. Safety analysis

Three different situations were considered, namely: (a) the safety of the building under vertical loading; (b) the safety of the building under vertical and wind loading; and (c) the safety of the building under vertical loading but assuming that there is no mortar rendering in the non-saturated masonry from the upper floors. Finally, a mesh dependence study is presented and the nonlinear analysis of the building subjected only to vertical loading is performed in order to verify the results obtained.

4.1.1. Loads

The vertical actions considered in the analysis include the self-weight of the structure and the imposed loads on the building arising from occupancy, as defined in Eurocode 1 [2002]. The specific weights of the materials used in the model are specified in Table 4. The imposed loads acting on the structures are dependent on the specific use of the building. According to Eurocode 1 [2002] the category of use of the building is Category A: areas for domestic and residential activities. The final imposed load values used for the present study are shown in Table 5.

The wind actions are also computed according to Eurocode 1 [2002], determined from the value of basic wind velocity of the region where the building is located. This value is obtained from the Brazilian code NBR 6123 [1988] and equals to 35 m/s. A complete itemization of the final values for wind loading used for the analyses on the vertical walls and on the flat roofs can be found in Ortega [2013].

4.1.2. Only vertical loading

A first nonlinear analysis of the building subjected only to its self-weight and live loads was carried out. First of all, the dead load (DL) and the live load (LL) were applied to the structure, according to the considered applicable load combination: 1.35DL + 1.5LL. After that, consecutive partial increments of the full load were imposed to the building. The solution procedure used the regular Newton Raphson method and an energy convergence criterion with a tolerance of 0.001, with the arc-length algorithm.

The results indicated that the initial value adopted for the compressive fracture energy needed correction, as the failure mode obtained from the numerical analysis was not in agreement with the observations. It is noted that the available data for the compressive failure of hollow clay block masonry is not available. Failure is much localized, taking place in the ground floor, at the connection between an internal wall and an opening, and occurs very explosively, i.e., it was not possible to have a follow-up of the collapse. As the real collapse of the building occurred after partial collapse of the foundation masonry walls, this result was not considered as representative of the global structural behavior of the building and the compressive fracture energy was subsequently increased aiming at obtaining a failure mode closer to reality. Figure 8 illustrates these results, it can be observed that the failure mode changed when the compressive fracture energy was modified, and collapse was due to crushing of the foundation saturated walls, matching better the observed failure mode. The

load-displacement diagrams resulting from the analyses, for a point at the top part of the building, are shown in Figure 9. It is possible to observe that the failure load is rather high, taking into account that the building actually collapsed for applied loads lower than the load combination adopted. Increasing the ductility factor *d* up to 6.4 mm allowed capturing the post-peak behavior, even if the collapse load for the ductility factors of 3.2 mm and 6.4 mm are rather close. Therefore, the results of the analysis for a ductility factor of 6.4 mm are the ones discussed next.

Additional results are shown in Figure 10, in terms of minimum principal strains, minimum principal stresses and maximum principal strains. As previously mentioned, the action that leads the collapse of the building is the crushing of the foundation masonry walls, specifically the walls located in the central part. Crushing results from reaching of the ultimate compressive strength. Figures 10a and 10b display the minimum principal stress distribution at the peak stage above ground and at the foundations. The areas above ground showing more stress concentration are localized close to the openings and balconies at the ground floor. In contrast, it can be observed that the stress distribution at the foundations is much homogeneous and the ultimate compressive strength has been reached by almost every wall. Figure 10c presents the minimum principal strains at the peak stage, which reach very high peak values.

Tensile damage starts arising in the structure at very early steps. After applying the full load (1.35DL + 1.5LL), some cracking is visible. The most sensitive regions to cracking are located at the openings, balconies and lintels, particularly at the ground floor. This evidence is in good agreement with what was observed during visual inspection, where cracks were already identified in those areas. The maximum principal strains at the peak stage are widely and intensely spread, see Figure 10d. The fact that, in reality, the building at collapse showed very little damage above ground confirms that the failure load is high and collapse

must occur at a much earlier step at the foundations. There is also cracking taking place at the foundations given the high compressive stresses to which these walls are subjected.

A simplified hand calculation allows a rough estimate of the safety factor of the structure. The estimated distributed force in the most loaded wall at the foundations $N_{applied}$ is around 99 N/mm. For a compressive strength f_c equal to 1.25 MPa and a wall thickness t equal to 190 mm it is possible to estimate the ultimate load of the wall N_{max} and the safety factor SF as:

$$N_{max} = f_c \cdot t = 237{,}5\ N/mm \rightarrow SF = \frac{N_{max}}{N_{applied}} = \frac{237{,}5}{99} = 2{,}4 \quad (1)$$

This value is close to the one obtained through numerical analysis and confirms that the compressive strength of the saturated masonry used for the calculation may not be accurate, as the safety factor is too high to justify failure even if it is also low from a code perspective, as no partial safety factor was considered on the material strength.

4.1.3. Vertical load and wind

Another set of nonlinear analyses were performed in the numerical model taking into account the wind actions (WL). Two different load combinations were considered, either considering the vertical load as beneficial or detrimental to the response: (a) 1.0DL + 1.5WL; and (b) 1.35DL + 1.05LL + 1.5WL. As expected for this type of buildings, the effect of the wind is not much relevant for the safety analysis and collapse still takes place at the foundation masonry walls in both cases, the weakest and most loaded part of the structure. However, as it could be expected, the most loaded walls are now those located in the area towards the building is leaning due to the wind actions. The ultimate load factor is almost the same as the previous one. The load-displacement diagrams for a point at the top of the building are presented in Figure 11. It is noted that the safety factor is highly increased for

one of the load combinations, which can be explained because the action that leads the collapse of the building is still the vertical loading and the multiplier of the dead load in this load combination is lower.

The results from the most severe (1.35DL + 1.05LL + 1.5WL) combination are presented in Figure 12 in terms of minimum principal stresses, minimum principal strains and maximum principal strains. Figure 12a illustrates the minimum principal stress distribution at the peak stage. The leaning of the building can be clearly identified, as the highest values of compression accumulate on one side of the building leading to the collapse mechanism previously described. The leaning effect can also be easily recognized in Figure 12b, which shows the minimum principal strains. Finally, the wind actions highly enhance the tensile damage and cause additional relevant cracking due to the suction effect, especially at the upper part of the building, see Figure 12c.

4.1.4. Vertical loading without rendering

A final safety analysis was performed on the building based on the hypothesis that the upper floors masonry had no rendering. The effect of the mortar rendering in the compressive behavior of the masonry was confirmed in the laboratory testing. The analysis aimed at quantifying the safety of the building if there were no rendering or if the rendering had no influence on the strength of the masonry, as usually done for design. The analysis was carried out according to the same load combination used in the first analysis (1.35DL + 1.5LL).

First of all, the mechanical properties of the non-saturated masonry needed to be updated to represent the behavior of the masonry without rendering. The new masonry compressive strength was obtained from tests carried out by Mota [2006]. As only the mean value was available, the characteristic value was computed according to Eurocode 8 [2004], by dividing it by the confidence factor. The remaining nonlinear properties were reduced

accordingly, as they can be calculated directly from the compressive strength, and shown on Table 6. Properties non-dependent from the compressive strength were kept the same.

The load-displacement diagram is presented in Figure 13. As it could be expected, the load factor is significantly reduced to 1.71, which is a reduction of 35% and provides a rather low safety factor, as the usual value for the material safety factor in masonry according to Eurocode 6 [2005] is about 2.0-2.5. Moreover, the failure mode is also modified and takes now place at the ground floor and not in the foundation, showing a much brittle behavior. The response of the structure is almost linear until collapse, which occurs very explosively close to an opening. The results are shown in Figure 14 in terms of incremental displacements and minimum principal strains. At failure, there is barely any compressive damage at the foundations, which is mostly concentrated at the ground floor.

4.1.5. Mesh dependence study

The elements used in the adopted model are rather large and, thus, an over brittle response could be expected. Consequently, a mesh dependence study was conducted to assess the influence of the mesh in the results. A second refined model presented in Figure 15 was constructed and this time only quadrilateral isoparametric 8 nodes curved shell elements (CQ40S) were used. The new mesh has 99,360 nodes and 33,752 elements. The elements at the base are again fully restrained and the same four different materials are applied. The total mass of the model is the same: 1020 tonnes.

The safety analysis of the building subjected only to vertical loading (1.35DL + 1.5LL) was re-run with the refined model. Results show very little differences with those obtained from the original model. Figure 16 illustrate the load-displacement diagrams resulting from the analysis, for the same point at the top part of the building used in the previous diagrams. It is possible to observe that the response of the building is essentially the

same as the one obtained with the original model, just slightly stiffer, and the variation in terms of the peak load is below 5%. Moreover, it is still very sensitive to the variation of the compressive fracture energy, and this had to be increased again in order to obtain a failure mode which was more consistent with the failure mode observed in reality. A final ductility factor *d* of 6.4 mm was needed to be used again in order to capture the post-peak behavior of the structure. The failure mode obtained for this value is due to crushing of the foundation masonry walls and the safety factor (LF=2.72) is still too high to justify the collapse of the building.

As a conclusion, and in view of the similarity between the results obtained from both models, the validity of original one can be confirmed and its results are assumed to be reliable and representative of the actual structural behavior of the studied building.

4.1.6. Conclusions

On December 2007, the building under analysis collapsed and sank more than one meter because of the failure of the saturated masonry walls at the foundations. The building did not entirely collapse due to the existence of tie-beams at every floor level. In fact, the floors above ground remained in fairly good condition, showing little damage except in some localized parts. These localized parts of the building may have collapsed due to the dynamic effects resulting from the impact of the building to the ground. The results of the analysis considering only vertical loading show good agreement between the crack patterns observed in reality and the damage achieved numerically at the current condition (*LF*=1). The failure mode seems to be well matched, even though the safety factor obtained does not justify the collapse observed in reality. The foundation walls must collapse at a much earlier stage than the one predicted by the model.

4.2. Sensitivity analysis

The inconsistency between the numerical results and the actual failure may be explained by the material properties used in the analysis, specifically for the saturated masonry. The authentic material properties must be highly deteriorated due to the continuous exposure to water, either due to contamination or leaching, and, therefore, they must be lower than the properties adopted. Furthermore, long-term effects, such as temperature changes and creep, may have had also influenced the behavior of the masonry. A collapse assessment and a sensitivity analysis are, therefore, relevant and are presented next.

4.2.1. Reference analysis

The reference analysis used for the sensitivity analysis and collapse assessment used the material properties described in Section 3, taking into account the corrections applied in Section 4.1.1., and considered the condition of the building at failure, using the load combination: 1.0DL + 0.3LL. The load-displacement diagram for a point at the top of the building is given in Figure 17. The load multiplier at collapse is 4.12, which is rather high and confirms that the building should not have collapsed under normal conditions and other factors must have played a decisive role in the observed collapse. A second analysis taking into account the geometrical nonlinearity of the structure was also performed because buckling of the most loaded walls at the foundations levels was detected at failure. However, results were very similar to the results of the reference analysis, concluding that the geometrical nonlinearity (unless of severe imperfections being present) has not a relevant influence on the failure mode of the structure with the exception of the post-peak behavior, which is slightly more brittle after the peak load, as it can be observed in the load-displacement diagram.

The results of the reference analysis at peak load are given in Figure 18, in terms of incremental and total displacements, minimum principal stresses, minimum principal strains and maximum principal strains. It is noted that the results are shown separately for the foundations and for the building above ground. The failure mode was previously discussed and occurs due to crushing of the foundation masonry walls.

4.2.2. Collapse assessment

In order to evaluate why the building fell in reality, the possible long-term effects on the saturated masonry were introduced. An analysis was performed based on the short-term creep tests carried out by de Carvalho [2010] and on the hypothesis that the compressive strength of the saturated masonry is critically reduced due to deterioration resulting from its environmental conditions. The compressive strength of the saturated masonry was reduced aimed at getting failure for a load factor equal to one. The long-term modulus obtained from the short-term tests was 133.4 MPa and the compressive strength needed to be reduced to 0.3 MPa in order to lower the load factor down to one, meaning a reduction of 76% of the value obtained from the test. The remaining nonlinear properties of the saturated masonry were computed according to the change in the compressive strength and are shown on Table 7. The properties non-dependent from the compressive strength were kept constant. The resulting load-displacement diagram is shown in Figure 19, where it is shown that indeed a unitary load factor was obtained. The reduction of the peak load as a result of the reduction of the compressive strength confirms that the structure is rather vulnerable to the possible deterioration of the masonry at the foundations. In addition, it can be observed that the reduction of the compressive strength and the reduction of the peak load factor are almost linearly correlated.

Collapse is still led by crushing of the foundation masonry walls. Crushing damage is now much extended along the foundations, as almost every wall has reached the ultimate compressive strength. However, while the damage at the foundations is considerably increased, the damage at the floors above ground is greatly reduced because the load is also much lower. Figure 20 shows the maximum principal strains above ground at the peak stage. This is in better agreement with what was observed in reality, as the building did not present much damage above ground at the time of collapsed, except for some cracking at the ground floor.

The results confirm that the initially assumed compressive strength must have been overestimated as they still match well the failure mode and the structure now collapse under the actual loading. It can be inferred that the long-term effects must indeed have had an influence on the structural response by deteriorating the masonry but the final value of the compressive strength, about 25% of the quasi-static value, seems too low to be justified only by creep. The reduction of strength is too severe so it may not be the only deteriorating agent undermining the masonry properties. Water must have also played a key role deteriorating the mechanical properties of the masonry for the structure to collapse. It is noted that the masonry has been under saturated conditions for more than ten years and there is not reliable information on the effect of this on the change of strength, due to salt crystallization, leaching or other chemical effects. A review of moisture and chemical effects on masonry and its degradation process is presented next.

4.2.3. Deterioration of masonry due to moisture and chemical effects

Brick masonry structures suffer important degradation when exposed to the physical and chemical effects of aggressive agents in the environment. Traditionally, research focus has been on the structural deterioration caused by direct mechanical aspects, but the decay

resulting from this interaction between environment and construction materials cannot be disregarded, as it causes a slow deterioration of the mechanical properties [Colla et al., 2013]. In the case under consideration, as previously pointed out, the level of the ground water table is very superficial, 0.75 m. and thus, the foundations masonry walls have been permanently saturated since they were built. Moreover, the building is close to the sea and sea salts may stem from the ground by rising damp. As water penetration and salts are the main catalysts for processes of degradation of the masonry, a brief review on the topic is justified.

The main physical-chemical degradation processes in which water and salts are involved include salt crystallization, leaching and sulfate or chloride attack. Moisture plays an important role in all these processes, whether as a transport medium introducing salts and other substances in the material and moving them inside, or as a solvent for the acid-soluble constituents of mortar and bricks. The internal pressures and stresses caused by the salt crystallization or by the formation of expansion compounds resulting from the reaction of sulfate or chloride salts with mortar components can be sufficiently large to originate severe cracking and spalling of the brick, leading to a loss of cohesion and strength of the material and to a decrease in the thickness of an element, resulting in a lower carrying capacity of the element itself. For more details about the process of degradation due to these three phenomena, the reader is referred to Lewin [1981], Berra et al. [1993], Binda and Baronio [1995], Larbi [2004] and Espinosa et al. [2008]. Further investigation is needed on the long-term influence of the water and chemical agents on the deterioration of the mechanical properties of the masonry of the studied building in order to verify if it can be responsible of such a critical reduction of strength.

4.2.4. Sensitivity analysis

A sensitivity analysis was performed, aiming at defining the parameters mostly influencing the results and confirming the conclusion made. The reference analysis was repeated for different material properties. Two groups were made: the first group included the elasticity modulus (E), the compressive strength (f_c) and the tensile strength (f_t); the second group included the compressive fracture energy (G_{fc}) and the mode I fracture energy (G_{fI}). For the first group, a closer estimation of the parameters was assumed and the values of the original analysis were multiplied and divided by a factor of 2.0. For the second group, no experimental data was available and a higher variance of experimental data is usually found in the literature. Therefore, it was assumed that a close estimation of the parameter was more difficult and the values of the original analysis were multiplied and divided by a factor of 5.0.

The sensitivity analysis was applied to the masonry, both saturated and non-saturated simultaneously, understanding that the basic property changes in the masonry affect both types. A total of ten analyses were carried out. The results are shown in Figure 21 in terms of load-displacement diagrams and a comparison of the peak loads is given in Table 8.

From the load-displacement diagram illustrated in Figure 21a, it can be observed that the influence of the elasticity modulus on the structural response of the building affects primarily the elastic stiffness and thus, the deformation is much increased or decreased according to the variation of this parameter. As the response of the structure is fundamentally linear until very high load factor values, the structure is very sensitive to the variation of this parameter in terms of deformation. However, the results are only very slightly sensitive in terms of peak loads, the difference to the reference value is around 5%, and the failure mode remains the same. The variation of the tensile strength and mode I fracture energy, have almost no influence on the results, as it could be expected, given the compressive dominated failure, see Figure 21b and Figure 21c. The differences to the peak load are smaller than 1% and the failure mode did not vary.

On the other hand, results are very much sensitive to the variation of the compressive strength and the compressive fracture energy. Figure 21d confirms that the structural response of the building is mostly dependent of the compressive strength of the masonry. The differences in terms of peak loads are very large, around 50%, showing again that the reduction of the compressive strength and the reduction of the peak load factor are almost linearly correlated. The failure mode varied in both analyses, when the compressive strength was reduced to half, the structure behaves almost ideally in compression and, oppositely, when the compressive strength was doubled, collapse became much more brittle, being the structural response practically linear until collapse. Failure occurs very explosively at the ground floor. Correspondingly, the variation of the compressive fracture energy illustrated in Figure 21e, has a large influence on the failure mode of the structure. This influence was previously discussed in Section 4.1.1, where the ductility index was modified in order to obtain a less explosive and localized collapse. In accordance with the previous results, the collapse is much brittle when the compressive fracture energy is reduced and the structural response is almost linear until collapse. The difference in terms of peak load is rather large (over 20%) because the structural response is controlled by the brittle failure taking place close to an opening at the ground floor. In contrast, the structure behaves almost ideally in compression when the compressive fracture energy is increased. Failure mode did not vary and the difference to the reference peak load is quite low (3.8%).

The results show that the structure is sensitive to the variation of the parameters in compression, particularly to the compressive strength and less to the compressive fracture energy, which was expected given the compressive dominated failure.

4.2.5. Earth pressure on the foundation masonry walls

Concerning the foundations, the space between the ground floor and the continuous footing is only partially filled for this particular set of buildings, leaving the most part empty. This is a common local construction practice known as ‘caixão vazio’, which makes the structure vulnerable to the lateral earth pressure.

This lateral thrust leads to an eccentricity of the upper load in the walls and it was deemed appropriate to perform an additional analysis taking into account the earth pressure on the foundation walls in order to evaluate its influence on the collapse of the building. The analysis was carried out according to the same load combination used for the safety analysis but including the lateral earth pressure (P): 1.35DL + 1.5LL + 1.5P. It is noted that some codes would consider this load as a dead load, not a live load. In the present case, given the uncertainty about the level of the earth for all the buildings, it was considered more reasonable to consider it as a live load.

The load-displacement diagram for a point at the foundation masonry walls that presents the maximum buckling is presented in Figure 22. It is noted that the load factor is reduced to 2.21, which means a reduction of 18%. This demonstrates that this pressure might have helped to lead to the building collapse. However, it again does not justify the failure of the building. Given the compressive dominated failure of the masonry walls, the arching effect in the vertical direction that could have been assumed to mitigate this effect, has only minor influence.

The failure mode for this new analysis still occurs at the foundation masonry walls but now takes place at the larger perimeter walls where the earth pressure, as shown in Figure 23.

5. Conclusions

A safety analysis and a sensitivity analysis of a box-building in Recife were successfully completed in order to understand the global structural behavior of the building

and the importance of each material parameter on it. The results achieved numerically at the current condition (LF=1) show good agreement with the damage observed in the structure and seem to be representative of the real behavior of the building. However, the safety factor obtained did not justify the collapse observed in reality.

Results indicated that the building must not have collapsed under normal loading conditions and therefore, one hypothesis of the reasons for the collapse was suggested. The failing part of the building was indeed at the foundation masonry walls, which were confirmed through visual inspection to be in direct contact with water and, thus, saturated. For this reason, the material properties used initially for the foundation saturated masonry were assumed to be incorrect and the compressive strength was assumed to be overestimated. The compressive strength for the building required to explain failure had to be reduced by ¾. This severe reduction can hardly be justified by the effect of creep and saturation, so it was concluded that chemical attacks must have had a great influence on the critical deterioration of the masonry, due to salt crystallization, leaching, sulfate attack or other effects. The fact that the foundations are built using the 'caixão vazio' construction practice, i.e. leaving the space between the ground floor and the continuous footing partially empty, makes the structure vulnerable to the lateral earth pressure. Results show that the earth pressure reduces the ultimate load factor by 18%, which is not enough either to justify failure by itself.

There is an urgent need to find a solution to the problem of this type of buildings in Brazil, given the precarious conditions of many of them. It is noted that it is difficult to predict the failure in advance as the floors above ground do not present much damage at collapse. Indeed, most of the collapsed buildings fell without previous warning. The problem involves more than 250,000 people and there is still a lack of methodology to assess the safety, and to strengthen and repair these buildings. The results obtained give valuable hints for understanding the involved phenomena and for addressing possible structural

strengthening, as the areas more sensitive to the structural problems have been identified. Solutions for strengthening should specifically address the foundations, where the failing parts of the building are localized.

Further investigation is needed and a number of areas for further research have been recognized: (a) Even if the results obtained showed that failure cannot be justified only by creep, the execution of a time-dependent analysis of the structure, by incorporating creep phenomena, chemical degradation and lower fracture energy in compression is encouraged; (b) Further research on the mechanical characteristics and structural behavior of this masonry type. In particular, the influence of the water and chemical agents on the deterioration of the mechanical properties of the masonry must be studied; (c) Research on interventions for the strengthening and repairing of these buildings. General criteria for the safety evaluation should be prepared so the need for intervention can be properly addressed. A general plan of action, including priorities, catalogue of solutions and required investment is a must.

References

Ahmad, S., Irons, B. M., Zienkiewicz, O. C. [1970] "Analysis of thick and thin shell structures by curved finite elements." International Journal for Numerical Methods in Engineering, 2(3), pp. 419-451, July-September.

Ademovic, N., Hrasnica, M., Oliveira, D. V. [2013] "Pushover analysis and failure pattern of a typical masonry residential building in Bosnia and Herzegovina." Engineering Structures, 50(3), pp. 13-29, May.

Araujo, A. S., Lourenço, P. B., Oliveira, D. V., Leite, J. [2012] "Seismic Assessment of St James Church by Means of Pushover Analysis - Before and After the New Zealand Earthquake." The Open Civil Engineering Journal, 6, (Suppl 1-M5), pp. 160-172.

Berra, M., Fatticcioni, A., Binda, L., Squarcina, T. [1993] "Laboratory and in-situ measurements procedure of the decay of masonry surfaces." In 6th International Conference on Durability of Building Materials and Components, Omiya, Japan, October, eds. S. Nagataki, T. Nireki and F. Tomosawa, E&FN SPON, London, pp. 834-843.

Binda, L., Baronio, G. [1987] "Mechanisms of masonry decay due to salt crystallization." Durability of Building Materials, 4(3), pp. 227-240.

Calderini, C., Lagomarsino, S. [2008] "A continuum model for in-plane anisotropic inelastic behavior of masonry." ASCE Journal of Structural Engineering, 134(2), pp. 209-220.

Colla, C., Molari, L., Gabrielli, E., de Miranda, S. [2013] “Damp and Salt Rising in Damaged Masonry Structures: Numerical Modelling and NDT Monitoring.” Nondestructive Testing of Materials and Structures, Springer Netherlands, 6, pp. 1151-1156.

de Carvalho, J. M. [2010] “Investigação experimental e numérica aplicada a um edifício caixão da região metropolitana do Recife.” PhD Thesis, Universidade Federal de Santa Catarina, Brazil.

de Melo, M. J. A. C. [2007] “Análise de laudos emitidos sobre “prédios tipo caixão” da Região Metropolitana de Recife: causas apontadas para os desabamentos e interdições.” MSc Thesis, Universidade Católica de Pernambuco, Brazil.

de Oliveira, S. M. L C. [2009] “Influência da ação de agentes agressivos na capacidade resistente de blocos cerâmicos.” In 5º Congresso Internacional sobre Patologia e Reabilitação de Estruturas, CINPAR 2009, Curitiba, Brazil, June.

EN 1991-1-1. [2002] “Eurocode 1 – Actions on structures – Part 1-1: Densities, self-weight, imposed loads for buildings.” CEN, Brussels, Belgium.

EN 1991-1-4. [2002] “Eurocode 1 – Actions on structures – Part 1-4: General actions – Wind actions.” CEN, Brussels, Belgium.

EN 1996-1-1. [2005] “Eurocode 6 – Design of masonry structures – Part 1-1: General rules for reinforced and unreinforced masonry structures.” CEN, Brussels, Belgium.

EN 1998-1-3. [2004] “Eurocode 8 – Design of structures for earthquake resistance – Part 1-3: Assessment and retrofitting of buildings.” CEN, Brussels, Belgium.

Espinosa, R.M., Franke, L., Deckelmann, G. [2008] “Model for the mechanical stress due to salt crystallization in porous materials.” Construction and Building Materials, 22(7), pp. 1350-1367.

Gusmão, A. D., Calado, C. F. A., Nogueira, C. L., Silva, F. A. N., Oliveira, R. A., Cerqueira, S. O. [2009] “Diretrizes para Solução dos Problemas Relacionados aos Prédios Construídos em Alvenaria Resistente na Região Metropolitana do Recife.” EDUPE, Brazil.

Larbi, J.A. [2004] “Microscopy applied to the diagnosis of the deterioration of brick masonry.” Construction and Building Materials, 18(5), pp. 299-307.

Lewin, S.Z. [1982] “The mechanism of masonry decay through crystallization.” Conservation of Historic Stone Buildings and Monuments, National Academy Press, Washington, DC, pp. 120-144.

Lourenço, P. B. [1998] “Experimental and numerical issues in the modeling of the mechanical behavior of masonry.” In Structural Analysis of Historical Constructions, CIMNE, Barcelona, pp. 57-91.

Lourenço, P. B. [2000] “Anisotropic softening model for masonry plates and shells.” ASCE Journal of Structural Engineering, 126(9), pp. 1008-1016.

Lourenço, P. B. [2002] “Computations of historical masonry constructions.” Progress in Structural Engineering and Materials, 4(3), pp. 301-319, July.

Lourenço, P. B., Krakowiak, K. J., Fernandes, F. M., Ramos, L. F. [2007] “Failure analysis of Monastery of Jerónimos, Lisbon: How to learn from sophisticated numerical models.” Engineering Failure Analysis, 14(2), pp. 280-300, March.

Lourenço, P. B. [2009] “Recent advances in masonry structures: Micromodelling and homogenization.” in Multiscale Modeling in Solid Mechanics: Computational Approaches, eds. U. Galvanetto and M. H. Ferri Aliabadi, Imperial College Press, pp. 251–294.

Lourenço, P. B., Mendes, N., Ramos, L. F., Oliveira, D. V. [2011] “On the Analysis of Masonry Structures without box behavior.” International Journal of Architectural Heritage, 5(4-5), pp. 369-382, July.

Lourenço, P. B., Fernandes, F., Ramos, L. F., Carvalho, J., Roman, H. [2011] “Metodologia para diagnóstico e intervenção em edifícios correntes: habitação social no Porto e Recife.” in Seminário “Cuidar das Casas. A manutenção do património corrente.”, Porto, Portugal.

Marques, R., Pereira, J. M., Lourenço, P. B., Parker, W., Uno, M. [2013] “Study of the Seismic Behavior of the “Old Municipal Chambers” Building in Christchurch, New Zealand.” Journal of Earthquake Engineering, 17(3), pp. 350-377.

Mendes, N., Lourenço, P. B. [2009] “Seismic Assessment of Masonry “Gaioleiro” Buildings in Lisbon, Portugal.” Journal of Earthquake Engineering, 14(1), pp. 80-101.

Mota, J. M. F., Neto, G. N. A., Oliveira, R. A. [2006] “Influência da argamassa de revestimento na resistência à compressão axial em prismas de alvenaria resistente de blocos cerâmicos.” In XXXII Jornadas Sulamericanas de Engenharia Estrutural, Campinas, Brazil.

NBR 6123. [1988] “Forças devidas ao vento em edificações.” ABNT - Associação Brasileira de Normas Técnicas, Rio de Janeiro, Brazil.

Ortega, J. [2013] “Safety analysis of modern heritage masonry buildings: Box-buildings in Recife, Brazil.” MSc Thesis, University of Minho, Portugal.

Ramos, L. F., Lourenço, P. B. [2004] “Advanced numerical analysis of historical centers: A case study in Lisbon.” Engineering Structures, 26(9), pp. 1295-1310.

Roca, P., Cervera, M., Gariup, G., Pelà, L. [2010] “Structural Analysis of Masonry Historical Constructions. Classical and Advanced Approaches.” Archives of Computational Methods in Engineering, 17(3), pp. 229-325.

Rots, J. G. [1988] “Computational modeling of Concrete Fracture.” PhD Thesis, Delft University of Technology, The Netherlands.

TNO [2011] “DIsplacement method ANAlyser.” User's Manual, Release 9.4.4, Netherlands.

List of Figures

FIGURE 10 Results of safety analysis at the peak stage: (a) minimum principal stress at the foundations; (b) minimum principal stress above ground; (c) minimum principal strains (a crushing measure) at the foundations depicted on deformed mesh; and (d) maximum principal strains (a cracking measure) above ground depicted on deformed mesh.

FIGURE 11 Load-displacement diagrams for the combinations involving the wind load.

FIGURE 12 Results of safety analysis at the peak stage: (a) minimum principal stress at the foundations; (b) minimum principal strains at the foundations; and (c) maximum principal strains above ground.

FIGURE 13 Effect of masonry rendering on the load-displacement diagram for the floor live load combination.

FIGURE 14 Results of safety analysis at failure: (left) incremental displacements depicted on deformed mesh, note that collapse occurs at confined areas surrounding an opening; (right) minimum principal strains at the ground floor walls, where the damage is maximum.

FIGURE 15 New refined model used for the mesh dependence study.

FIGURE 16 Mesh dependence study: Load-displacement diagrams for a point at the top of the building for the floor live load combination, for both the original and the refined model, as a function of the compressive fracture energy.

FIGURE 17 Load-displacement diagram for the expected load at time of failure and consideration of geometrical non-linear effects.

FIGURE 18 Results of the reference analysis. The building above ground is depicted on the left side of the figure and the foundations on the right side. All the results refer to the peak load: (a) incremental displacements depicted on incremental deformed mesh; (b) total displacements depicted on total deformed mesh; (c) minimum principal stress depicted on total deformed mesh (results in MPa); (d) minimum principal strains depicted on total deformed mesh; and (e) maximum principal strains depicted on total deformed mesh.

FIGURE 19 Load-displacement diagram.

FIGURE 20 Maximum principal strains above ground (cracking) at peak load.

FIGURE 21 Influence of the material parameters on the load-displacement diagram of the building: (a) elasticity modulus; (b) tensile strength; (c) mode I fracture energy; (d) compressive strength; and (e) compressive fracture energy.

FIGURE 22 Load-horizontal displacement diagram for a point at the foundations where the buckling is maximum taking into account the lateral earth thrust. Note that the load-vertical displacement diagram for a point top of the building is also given as a reference, even if the diagrams cannot be compared.

FIGURE 23 Results of analysis taking into account the earth pressure at the peak stage: (left) incremental displacements depicted on deformed mesh; (right) minimum principal strains at the foundation walls.

FIGURE 1 Views of the building after the collapse.

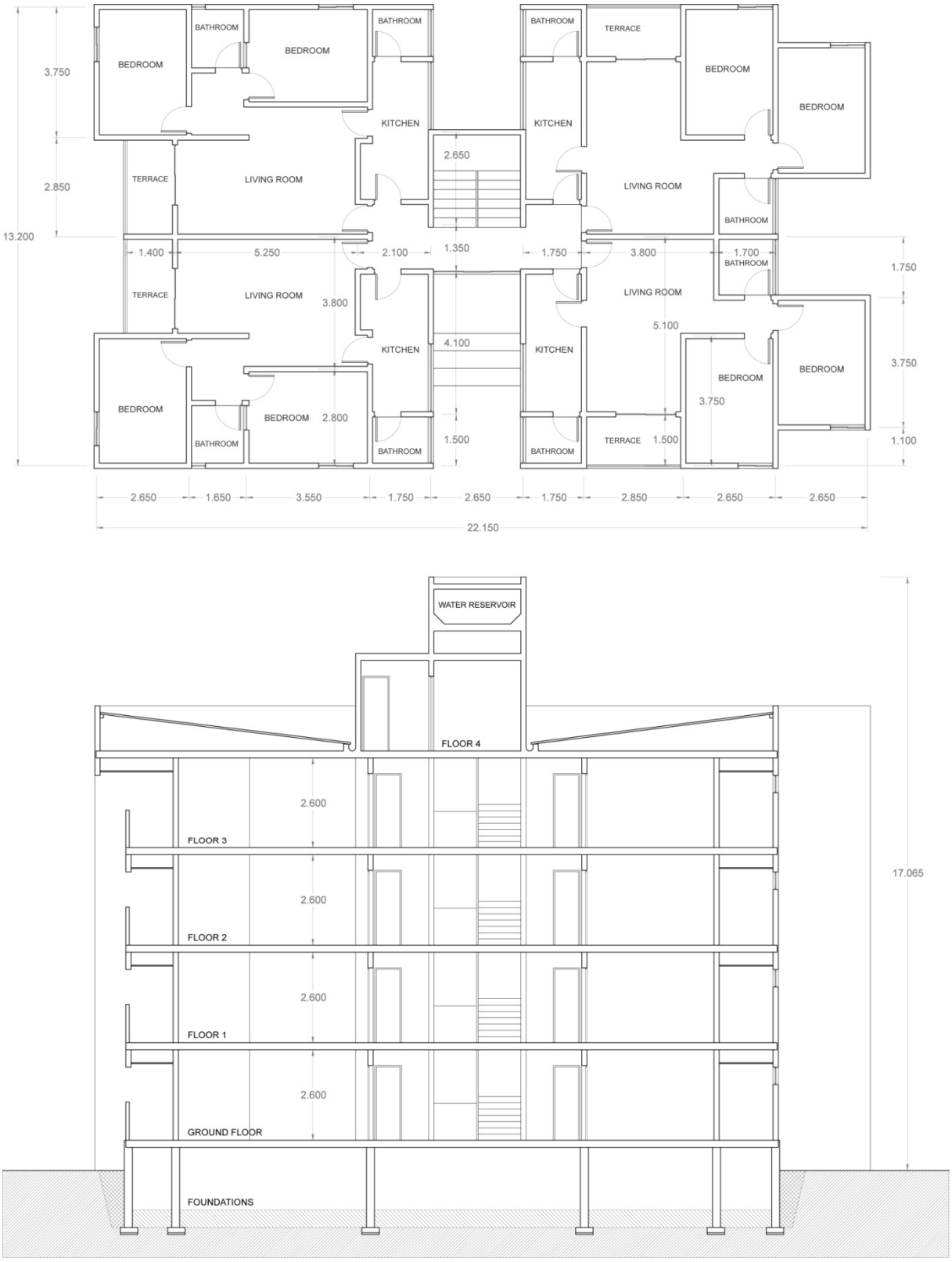

FIGURE 2 Architectural plans (dimensions in meters): (up) ground floor plan; (down) longitudinal section through the staircase.

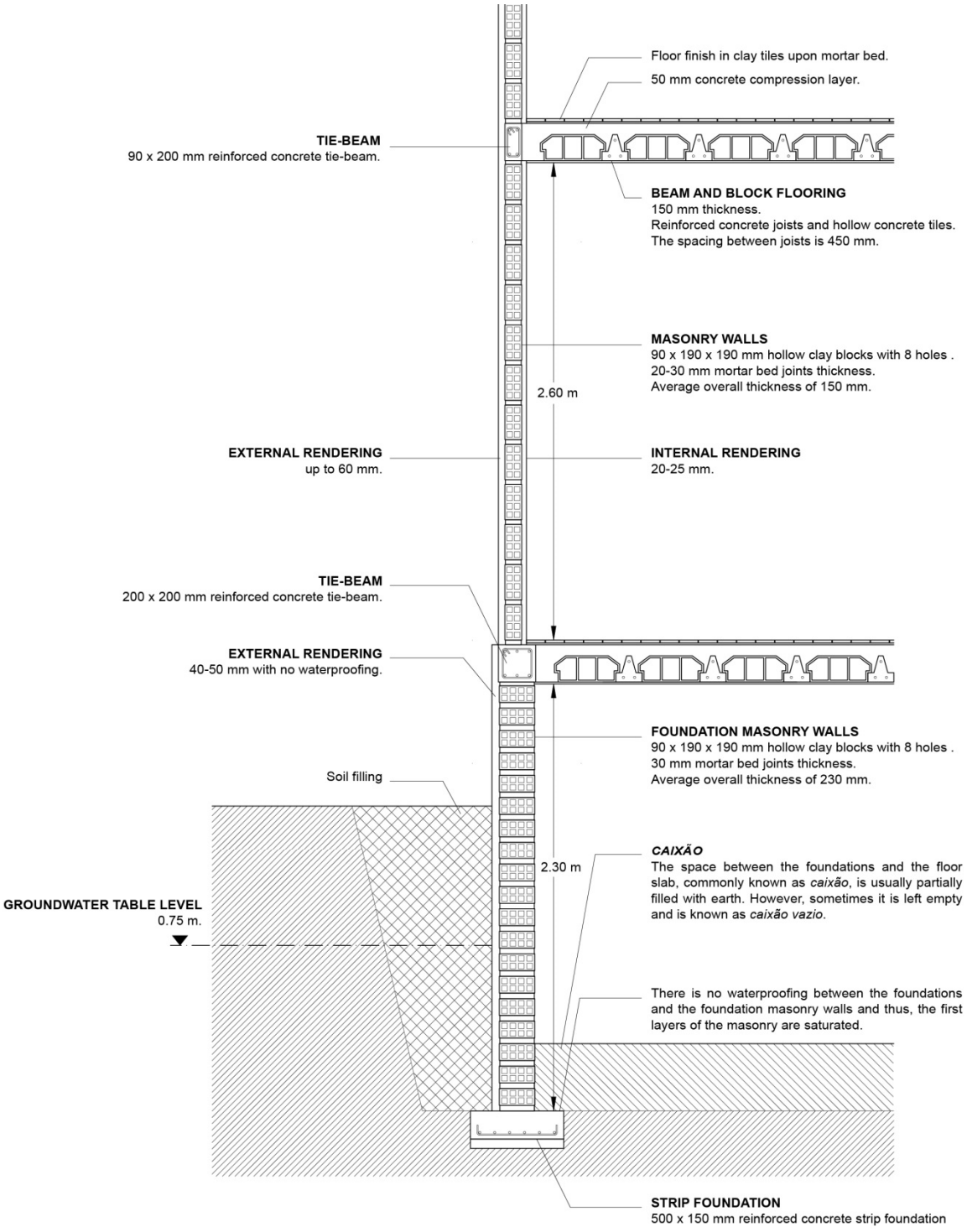

FIGURE 3 Construction details of the building.

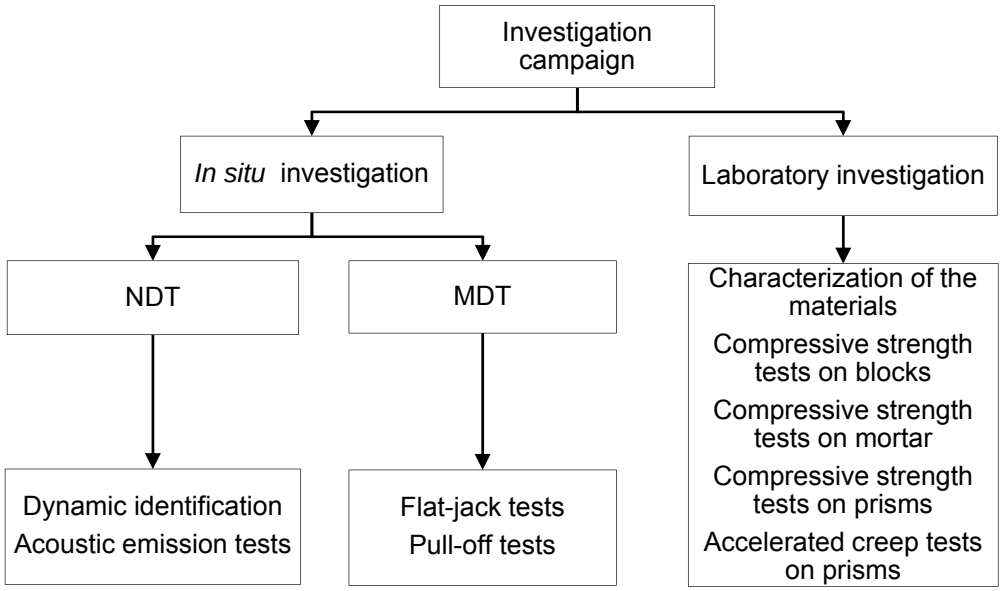

FIGURE 4 Investigation campaign carried out in the building [de Carvalho, 2010].

FIGURE 5 Failure mode of the masonry prisms tested.

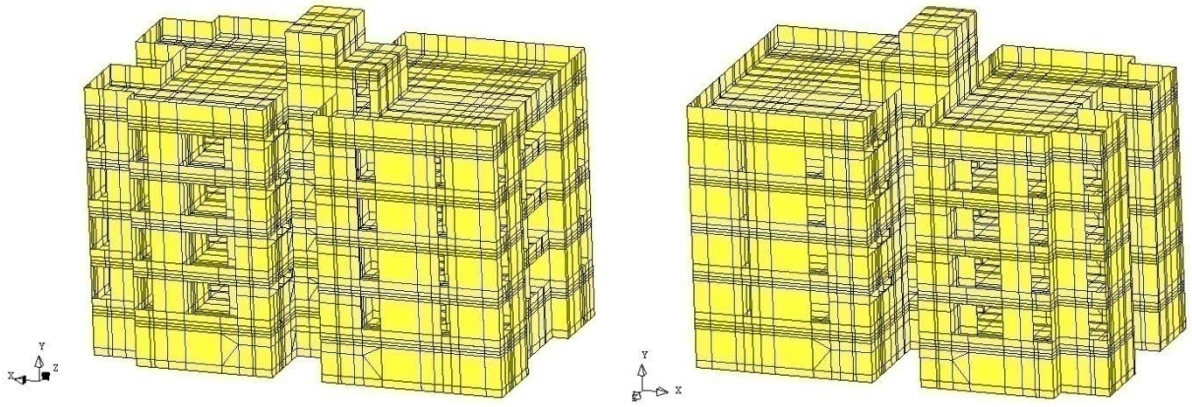

FIGURE 6 Model of the box-building.

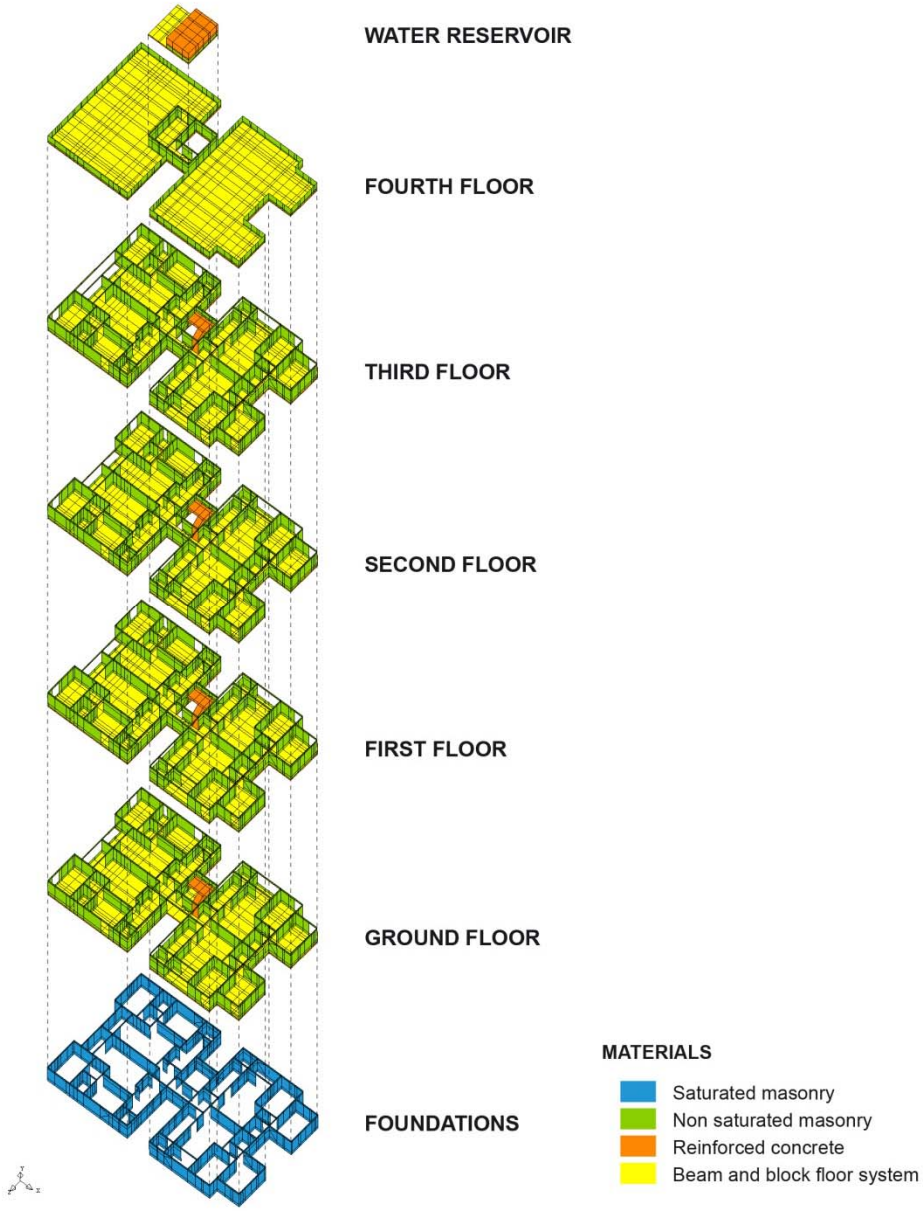

FIGURE 7 Numerical model: mesh categorized by floor levels and materials.

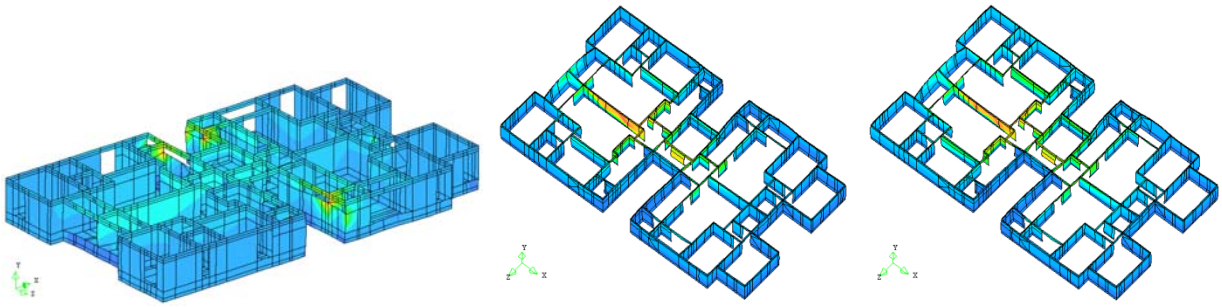

(a) (b) (c)

FIGURE 8 Incremental displacements at the ultimate stage depicted on deformed mesh: (a) unacceptable failure mode resulting from the first analysis (d=1.6 mm), consisting of failure of the masonry walls at the ground floor; (b) failure mode resulting from the second analysis (d=3.2 mm), consisting of crushing of the foundation walls; and (c) failure mode resulting from the third analysis (d=6.4 mm), consisting of crushing of the foundation walls.

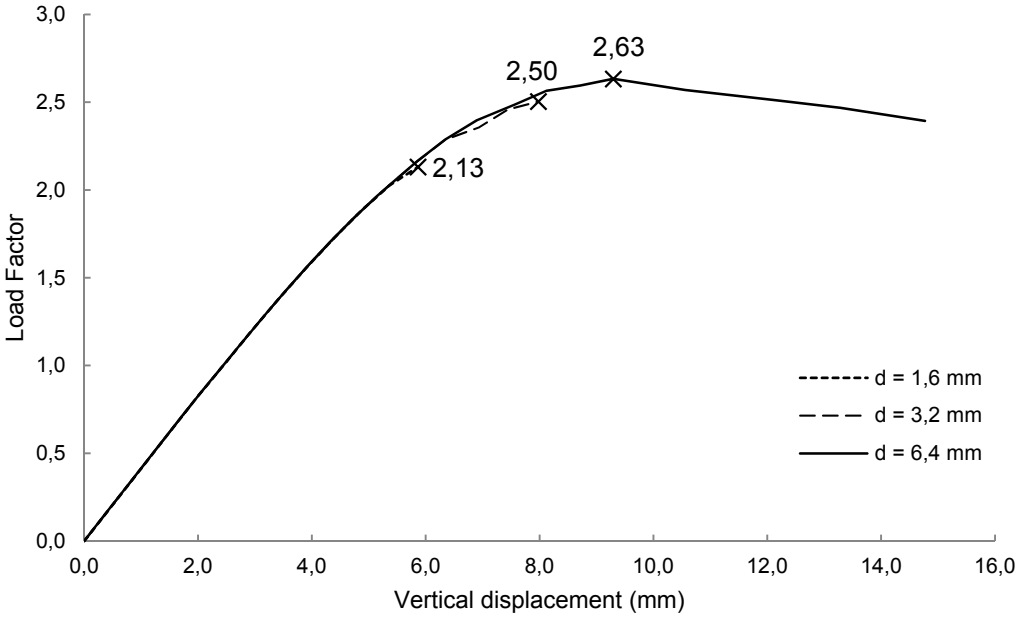

FIGURE 9 Load-displacement diagram for a point at the top of the building for the floor live load combination, as a function of the compressive fracture energy.

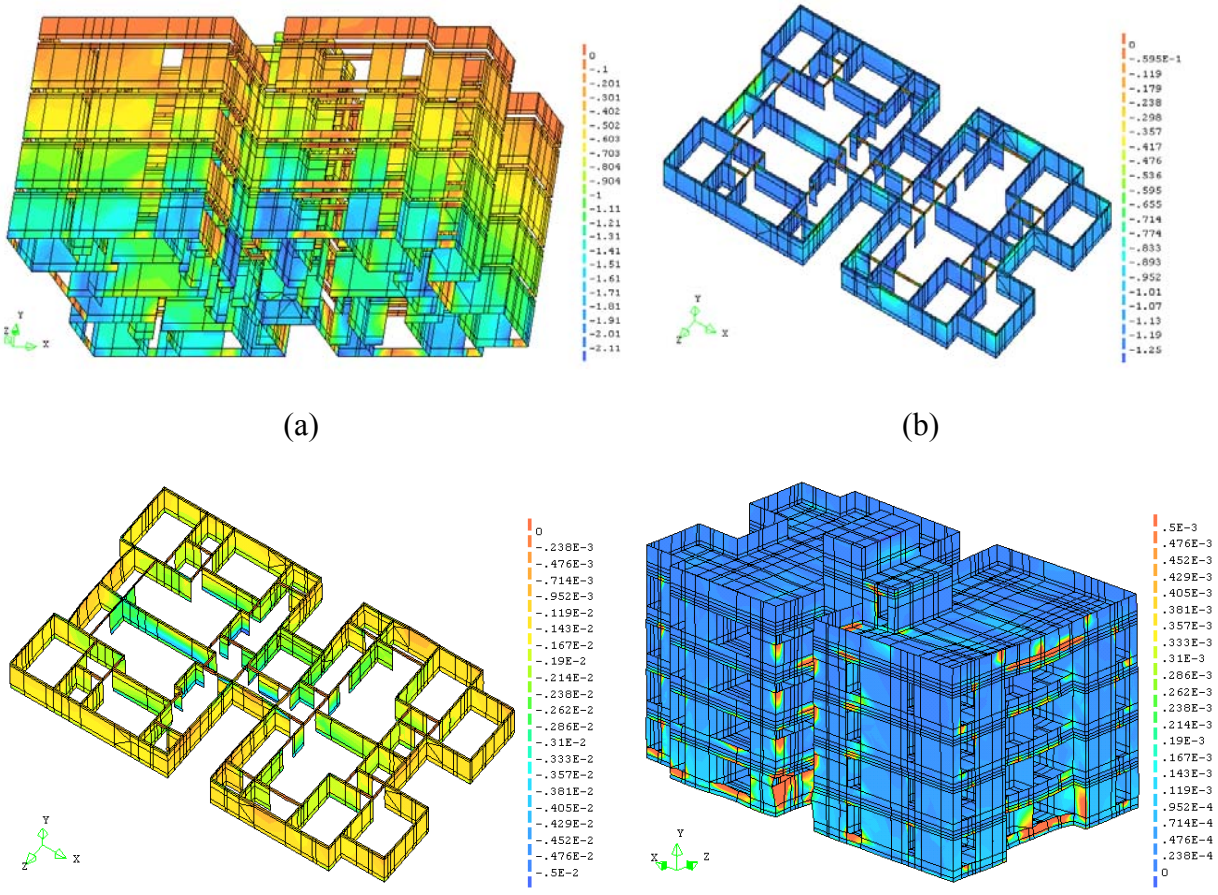

(a) (b)

(c) (d)

FIGURE 10 Results of safety analysis at the peak stage: (a) minimum principal stress above ground; (b) minimum principal stress at the foundations; (c) minimum principal strains (a crushing measure) at the foundations depicted on deformed mesh; and (d) maximum principal strains (a cracking measure) above ground depicted on deformed mesh.

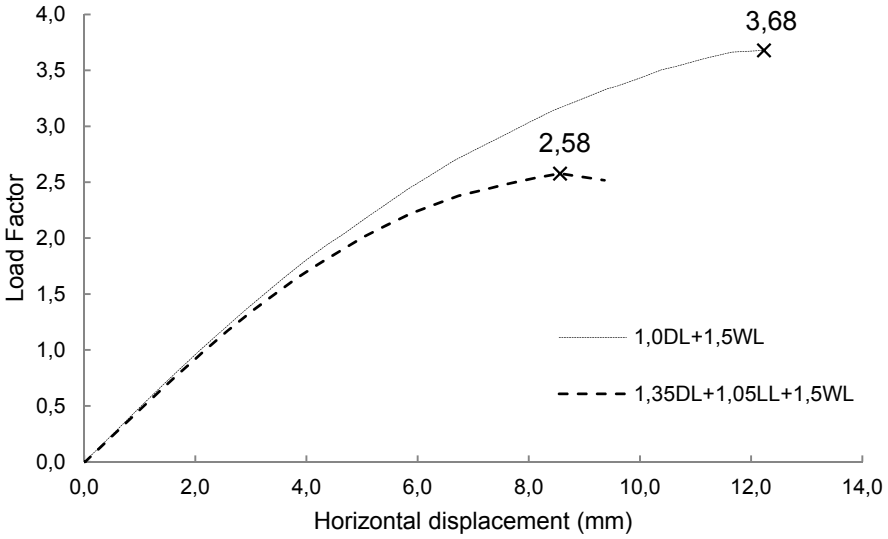

FIGURE 11 Load-displacement diagrams for the combinations involving the wind load.

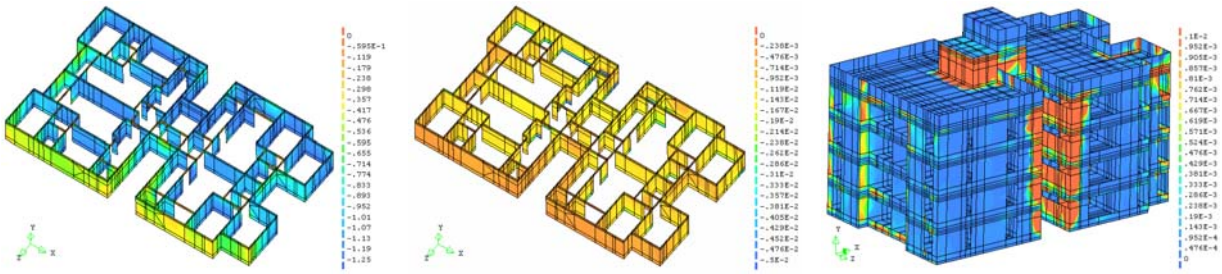

(a) (b) (c)

FIGURE 12 Results of safety analysis at the peak stage: (a) minimum principal stress at the foundations; (b) minimum principal strains at the foundations; and (c) maximum principal strains above ground.

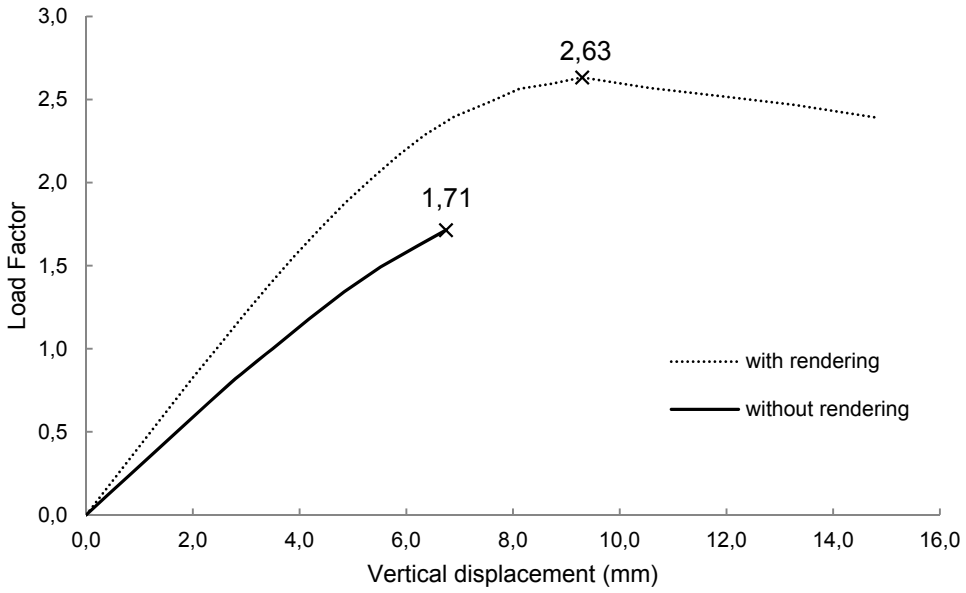

FIGURE 13 Effect of masonry rendering on the load-displacement diagram for the floor live load combination.

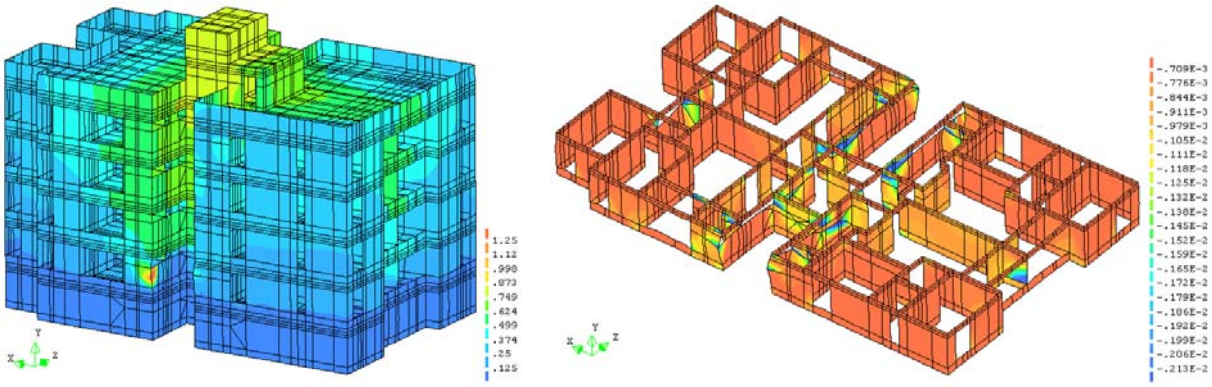

FIGURE 14 Results of safety analysis at failure: (left) incremental displacements depicted on deformed mesh, note that collapse occurs at confined areas surrounding an opening; (right) minimum principal strains at the ground floor walls, where the damage is maximum.

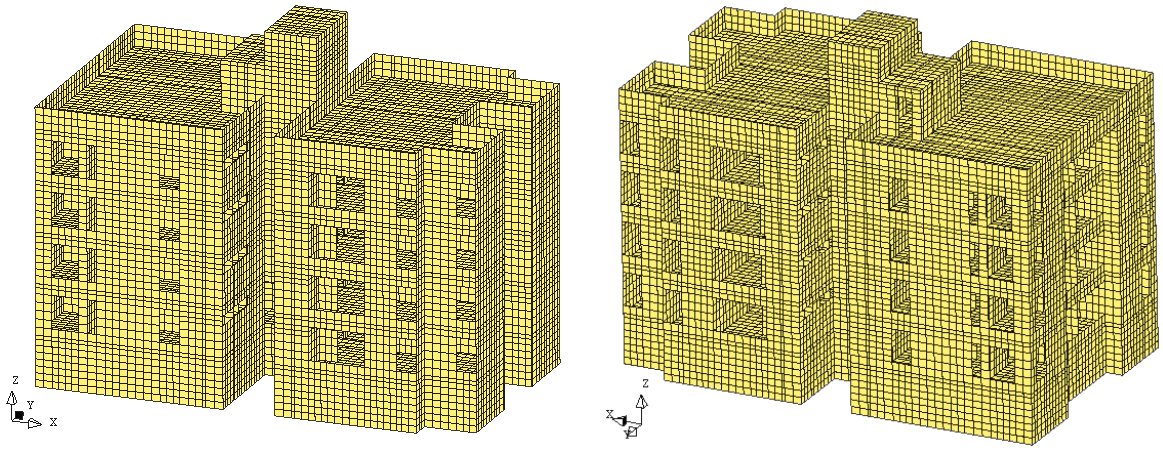

FIGURE 15 New refined model used for the mesh dependence study.

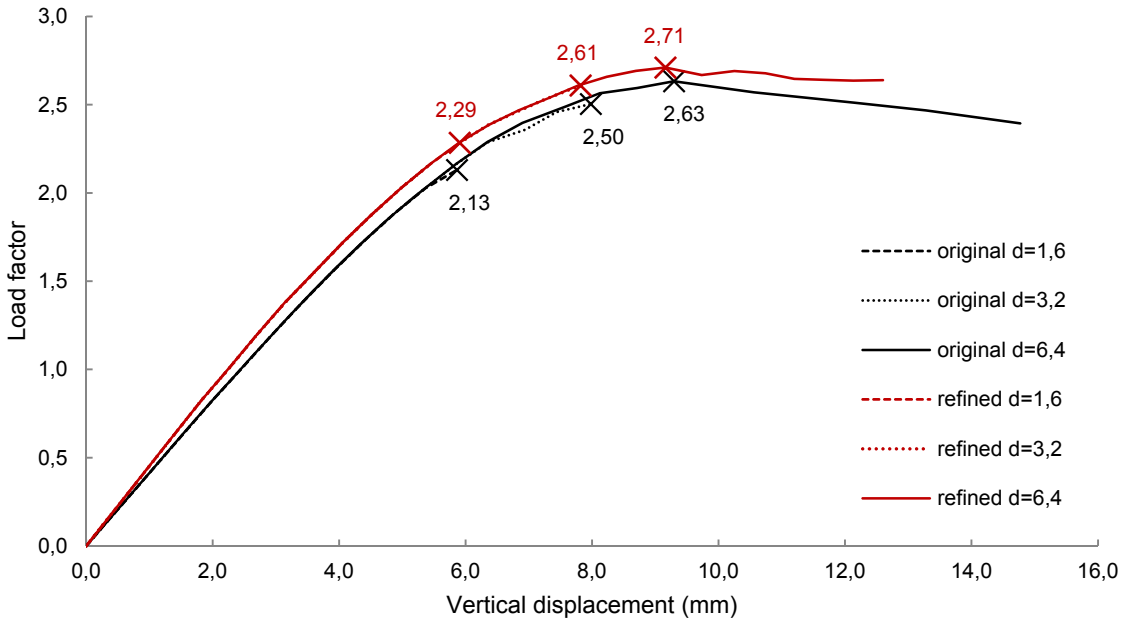

FIGURE 16 Mesh dependence study: Load-displacement diagrams for a point at the top of the building for the floor live load combination, for both the original and the refined model, as a function of the compressive fracture energy.

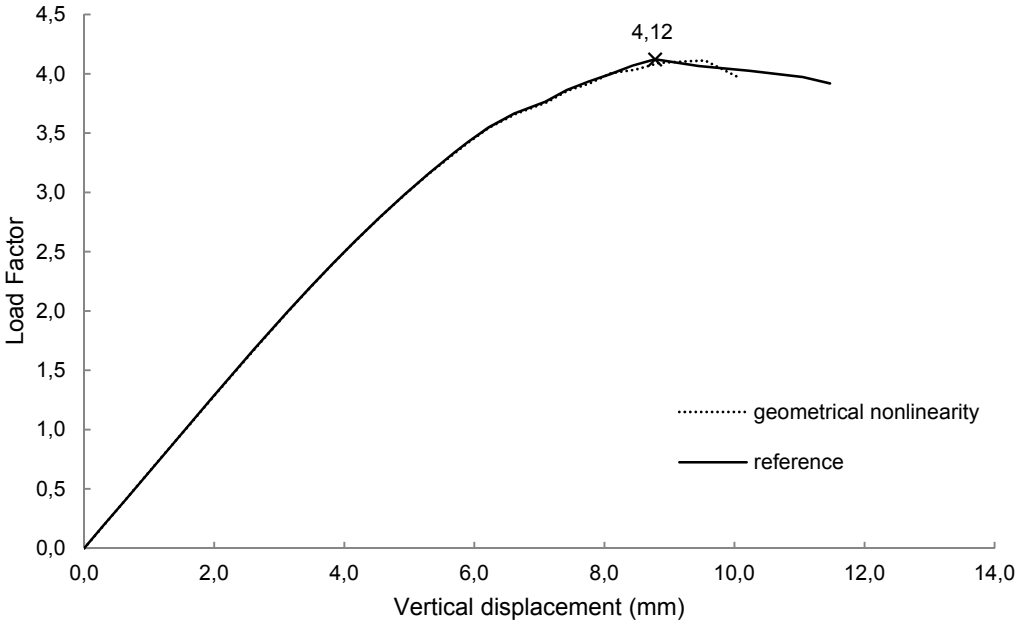

FIGURE 17 Load-displacement diagram for the expected load at time of failure and consideration of geometrical non-linear effects.

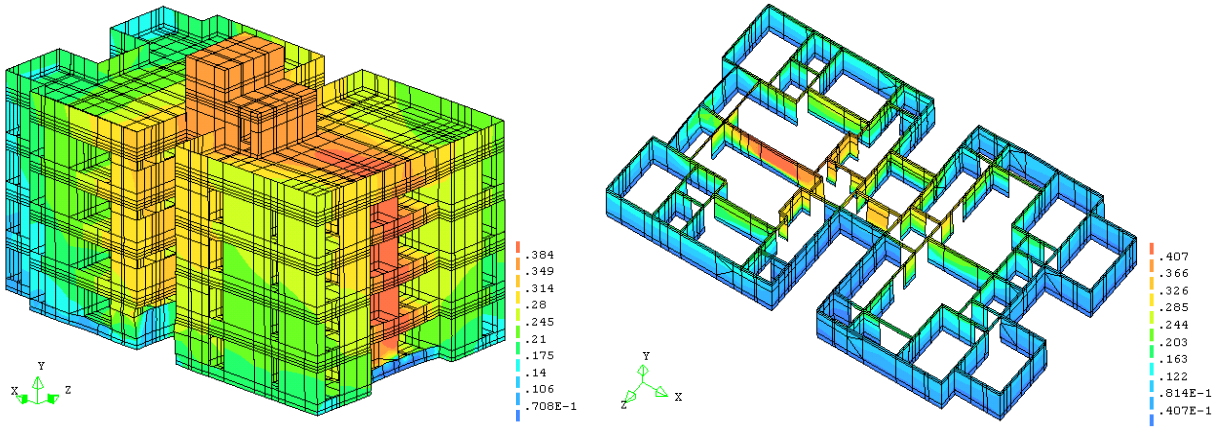
.384
.349
.314
.28
.245
.21
.175
.14
.106
.708E-1
.407
.366
.326
.285
.244
.203
.163
.122
.814E-1
.407E-1

(a)

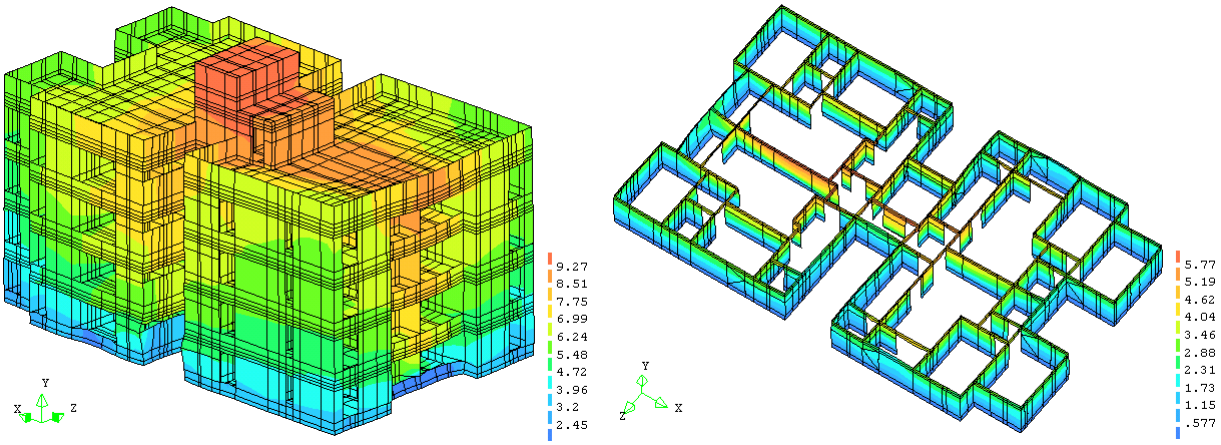
9.27
8.51
7.75
6.99
6.24
5.48
4.72
3.96
3.2
2.45
5.77
5.19
4.62
4.04
3.46
2.88
2.31
1.73
1.15
.577

(b)

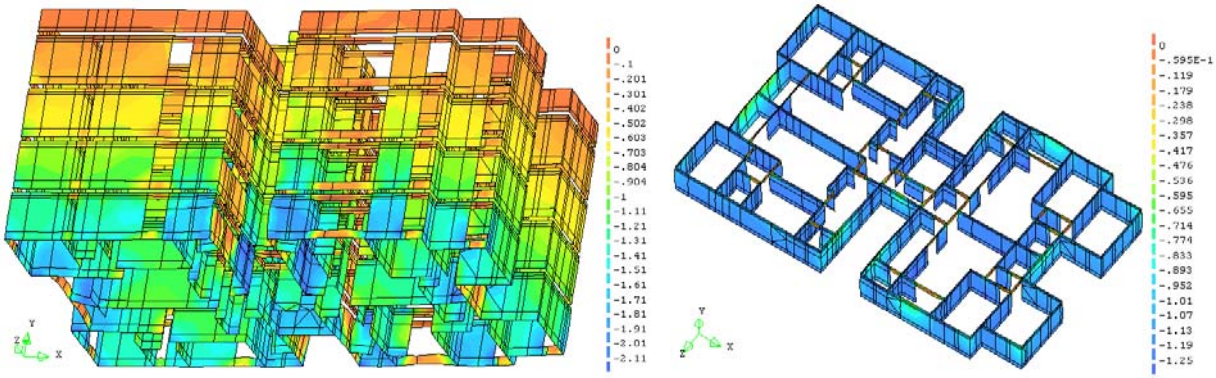
0
-.1
-.201
-.301
-.402
-.502
-.603
-.703
-.804
-.904
-1
-1.11
-1.21
-1.31
-1.41
-1.51
-1.61
-1.71
-1.81
-1.91
-2.01
-2.11
0
-.595E-1
-.119
-.179
-.238
-.298
-.357
-.417
-.476
-.536
-.595
-.655
-.714
-.774
-.833
-.893
-.952
-1.01
-1.07
-1.13
-1.19
-1.25

(c)

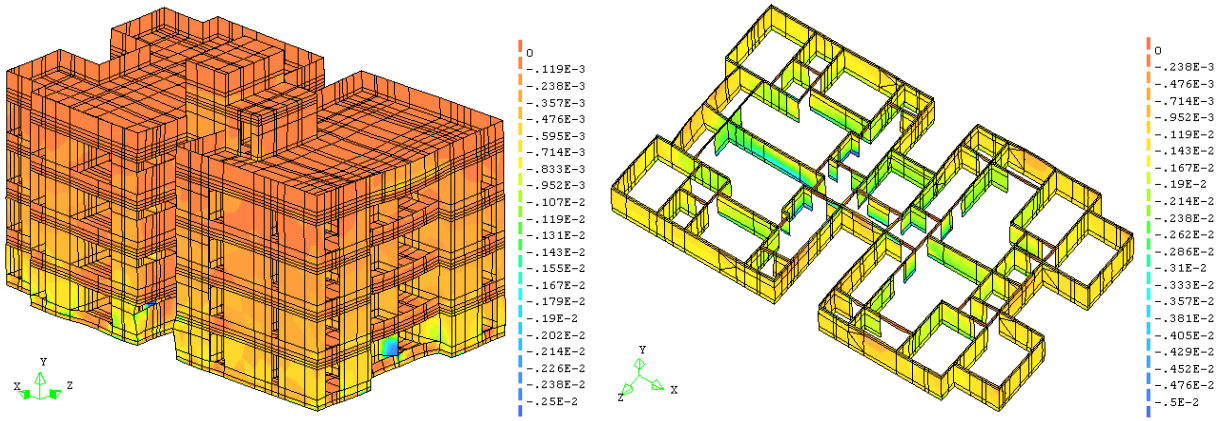

(d)

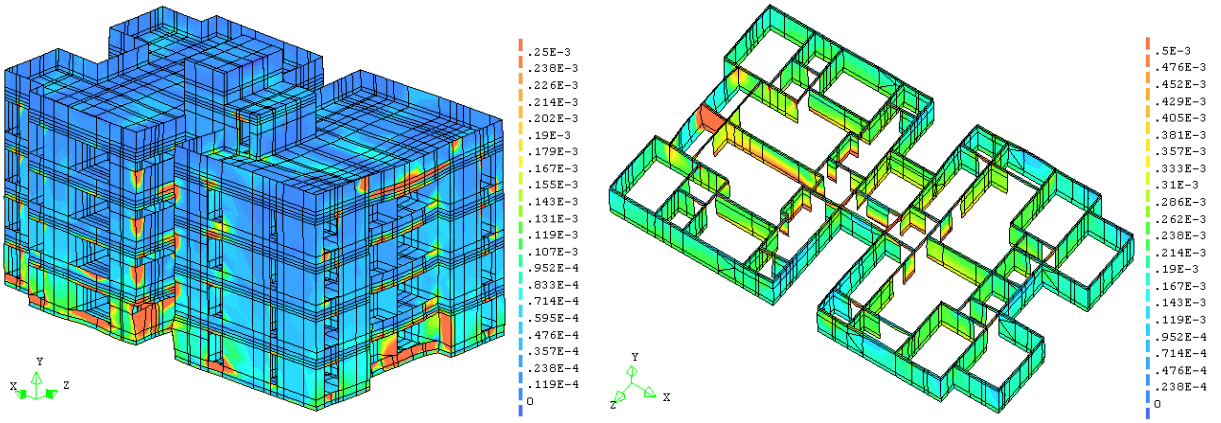

(e)

FIGURE 18 Results of the reference analysis. The building above ground is depicted on the left side of the figure and the foundations on the right side. All the results refer to the peak load: (a) incremental displacements depicted on incremental deformed mesh; (b) total displacements depicted on total deformed mesh; (c) minimum principal stress depicted on total deformed mesh (results in MPa); (d) minimum principal strains depicted on total deformed mesh; and (e) maximum principal strains depicted on total deformed mesh.

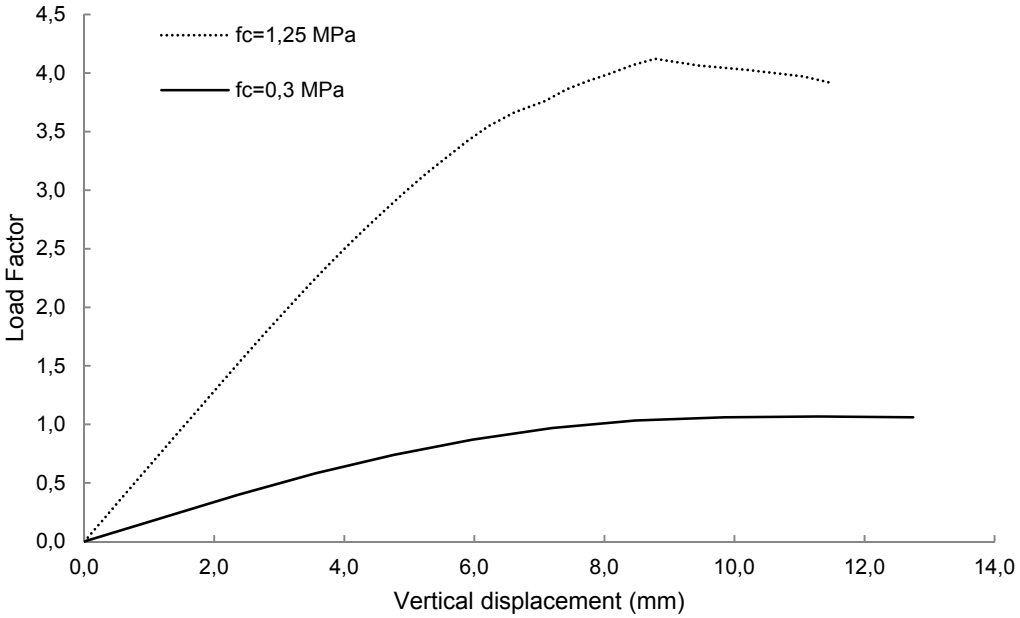

FIGURE 19 Load-displacement diagram.

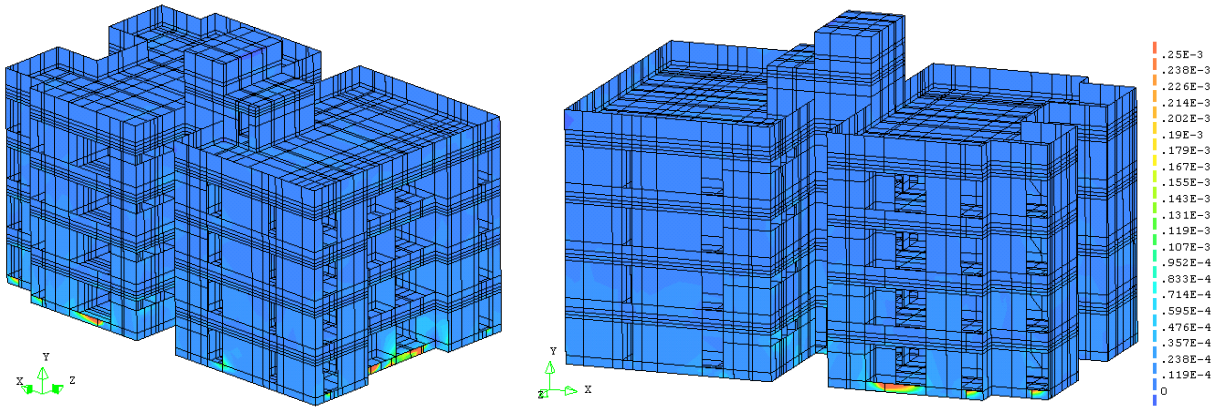

FIGURE 20 Maximum principal strains above ground (cracking) at peak load.

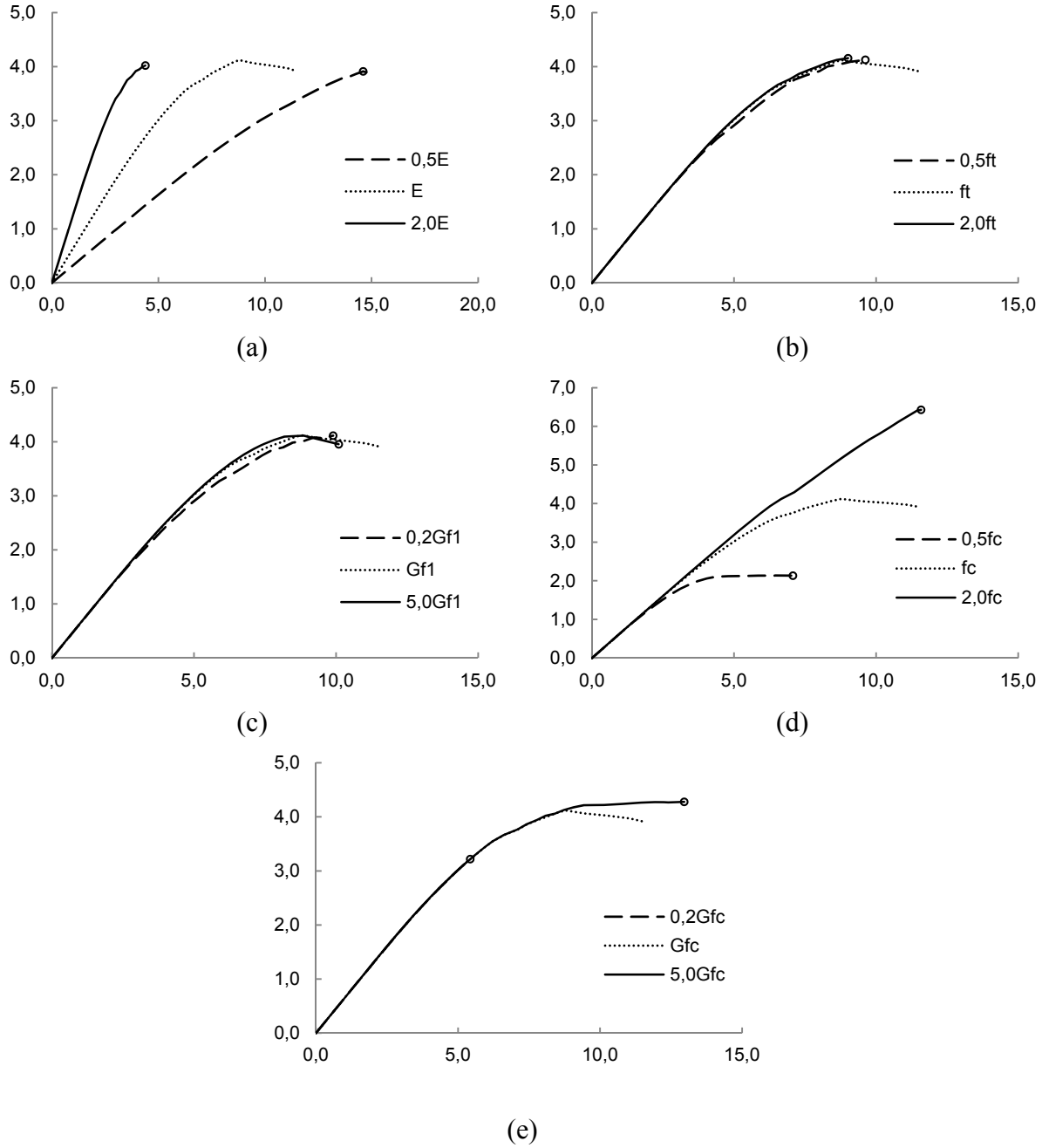

FIGURE 21 Influence of the material parameters on the load-displacement diagram of the building: (a) elasticity modulus; (b) tensile strength; (c) mode I fracture energy; (d) compressive strength; and (e) compressive fracture energy.

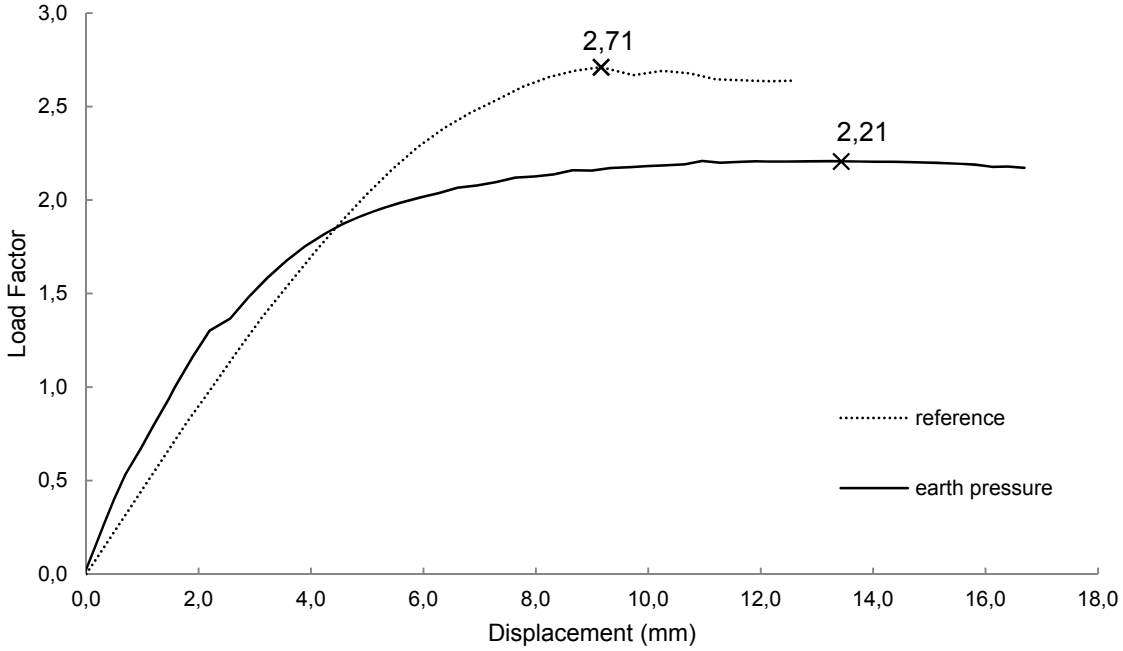

FIGURE 22 Load-horizontal displacement diagram for a point at the foundations where the buckling is maximum taking into account the lateral earth thrust. Note that the load-vertical displacement diagram for a point top of the building is also given as a reference, even if the diagrams cannot be compared.

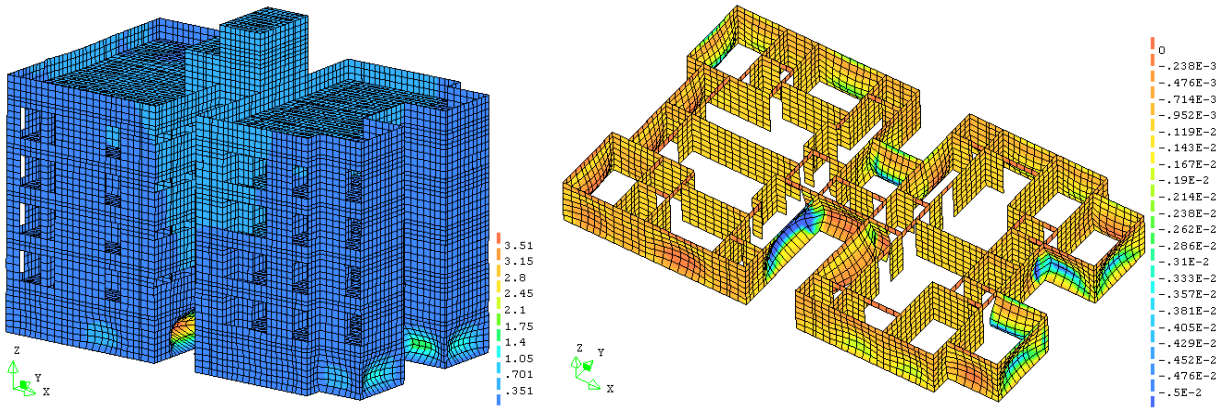

FIGURE 23 Results of analysis taking into account the earth pressure at the peak stage: (left) incremental displacements depicted on deformed mesh; (right) minimum principal strains at the foundation walls.

List of Tables

TABLE 1 Geometrical characteristics of the prisms tested at the University of Minho and results of compressive tests.

				Thickness				Compressive Strength (MPa)	Mod. of Elasticity (MPa)
	Prism	Height (mm)	Width (mm)	Rendering a (mm)	Block (mm)	Rendering b (mm)	Total (mm)		
Saturated	1	670.0	310.0	30.5	89.0	30.5	150	1.25	1034
	2	664.6	310.0	14.9	90.5	25.3	130	1.82	1036
	3	665.5	300.0	19.5	91.0	29.5	140	1.69	964
	Average	667.0	306.7	21.6	90.0	28.4	140	1.59	1168
	COV	0.4%	2%	37%	1%	10%	7%	19%	25%
Non-sat.	1	665.0	300.0	20.0	89.9	34.5	144	2.69	2558
	2	675.0	315.0	20.0	90.0	30.0	140	2.64	2973
	3	667.0	300.0	35.5	89.9	40.5	165	2.23	4392
	Average	669.0	305.0	25.2	89.6	35.0	150	2.52	3307
	COV	0.8%	3%	36%	1%	15%	9%	10%	29%

TABLE 2 Results from the dynamic calibration.

Experimental frequencies (Hz)		Numerical model					
		Frequencies (Hz)		Error (%)	Av. error (%)	Modulus of Elasticity	
Mode 1	4,1	Mode 1	4,2	2,7	6,9	Saturated (MPa)	2977
Mode 2	4,3	Mode 2	4,8	10,7		Non-sat. (MPa)	1052
Mode 3	5,4	Mode 3	5,0	7,4		Reduction (%)	10

TABLE 3 Nonlinear mechanical properties of the masonry.

	E (MPa)	v	f_c(MPa)	G_{fc} (N/mm)	f_t (MPa)	G_{f1} (N/mm)	β
Saturated	1052	0,13	1,25	2,00	0,125	0,012	0,05
Non-saturated	2977	0,13	2,10	3,36	0,210	0,012	0,05

TABLE 4 Specific weight of the materials used in the numerical model.

Material	Specific weight (kN/m^3)
Saturated masonry	13
Non-saturated masonry	13
Reinforced concrete	25
Beam and block floor system	23

TABLE 5 Imposed loads on the buildings.

Area	q_k (kN/m^2)
Floors	1,5
Stairs	3
Water reservoir	10

TABLE 6 Updated nonlinear mechanical properties of the non-saturated masonry (without rendering).

	E (MPa)	v	f_c (MPa)	G_{fc} (N/mm)	f_t (MPa)	G_{fl} (N/mm)	β
Non-saturated	2300	0,13	1,63	10,43	0,16	0,012	0,05

TABLE 7 Updated nonlinear mechanical properties of the saturated masonry.

	E (MPa)	v	f_c (MPa)	G_{fc} (N/mm)	f_t (MPa)	G_{f1} (N/mm)	β
Saturated	133.4	0,13	0.30	1,92	0,03	0,012	0,05

TABLE 8 Peak load factors obtained in the sensitivity analysis of the building. The reference peak load factor is 4.12. In brackets the difference to the reference value.

	First series of parameters		
	E	f_c	f_t
Divided by 2.0	3,91 (-5%)	2,14 (-48%)	4,13 (0%)
Multiplied by 2.0	4,02 (-2%)	6,41 (+55%)	4,16 (+1%)
	Second series of parameters		
	G_{fc}	G_{fl}	
Divided by 5.0	3,22 (-22%)	4,12 (0%)	
Multiplied by 5.0	4,28 (+4%)	4,11 (0%)	